Research Square

Preprints are preliminary reports that have not undergone peer review.
They should not be considered conclusive, used to inform clinical practice,
or referenced by the media as validated information.

BMP9 Promotes Hepatocellular Carcinoma Progression By Accelerating Cell Cycle through CKS1B Lactylation

Hong Tang

tanghong6198@wchscu.cn

West China Hospital of Sichuan University

Han Chen

Center of Infectious Diseases, West China Hospital of Sichuan University, Chengdu

Jianhao li

West China Hospital of Sichuan University

Ying-Yi Li

Department of Gastroenterology, Kanazawa University Hospital

Mingming Zhang

Center of Infectious Diseases, West China Hospital of Sichuan University, Chengdu

Jiayi Wang

Center of Infectious Diseases, West China Hospital of Sichuan University, Chengdu

Xia Zhu

Center of Infectious Diseases, West China Hospital of Sichuan University, Chengdu

Weixiu Li

Center of Infectious Diseases, West China Hospital of Sichuan University, Chengdu

Junpeng Zhou

Center of Infectious Diseases, West China Hospital of Sichuan University, Chengdu

Xiangnan Teng

Center of Infectious Diseases, West China Hospital of Sichuan University, Chengdu

Xuiemei Tao

Center of Infectious Diseases, West China Hospital of Sichuan University, Chengdu

Lichun Wang

Center of Infectious Diseases, West China Hospital of Sichuan University, Chengdu

Yujia Mao

Center of Infectious Diseases, West China Hospital of Sichuan University, Chengdu

Taro Yamashita

Kanazawa University

Kouki Nio

Kanazawa University

Article

Keywords: BMP9, HCC, Cell cycle progression, CKS1B, Lactylation

Posted Date: July 30th, 2026

DOI: https://doi.org/10.21203/rs.3.rs-10256326/v1

License: This work is licensed under a Creative Commons Attribution 4.0 International License.
Read Full License

Additional Declarations:
There is a duality of interest

Tables 1 to 2 are available in the supplementary files section.

BMP9 Promotes Hepatocellular Carcinoma Progression By Accelerating Cell Cycle through CKS1B Lactylation

Han Chen[1,2,3], Jianhao Li[1,2], Ying-Yi Li[4], Mingming Zhang[1,2], Jiayi Wang,[1,2] Xia Zhu[1,2], Weixiu Li[1,2], Junpeng Zhou[1,2], Xiangnan Teng[1,2], Xuemei Tao[1,2], Lichun Wang[1,2], Yujia Mao[1,2], Taro Yamashita[4], Kouki Nio[4], and Hong Tang*[,1,2,3]

1. Center of Infectious Diseases, West China Hospital of Sichuan University, Chengdu 610041, China;

2. Laboratory of Infectious and Liver Diseases, Institute of Infectious Diseases, West China Hospital of Sichuan University, Chengdu, 610041, China

3. Division of Infectious Diseases, State Key Laboratory of Biotherapy and Center of Infectious Diseases, West China Hospital of Sichuan University, Chengdu 610041, China

4. Department of Gastroenterology, Kanazawa University Hospital, Kanazawa 9208641, Japan;

*Correspondence:

Hong Tang, MD, Center of Infectious Diseases, Laboratory of Infectious and Liver Diseases, West China Hospital of Sichuan University, Chengdu610041, China. E-mail address: tanghong6198@wchscu.cn.

Abstract

Hepatocellular carcinoma(HCC) is a highly lethal malignant tumor, and bone morphogenetic protein 9(BMP9) has been implicated in the pathogenesis of liver diseases and HCC. This study aimed to investigate the role of BMP9 signaling in regulating lactylation and cell cycle progression in HCC. Our data revealed that elevated BMP9 expression in tumor tissues from HCC patients is significantly associated with poorer prognosis. Using mass spectrometry, we identified that among cell cycle-related proteins, the lactylation modification at the 4th lysine residue of Cyclin-dependent kinase regulatory subunit 1B(CKS1B) is the most significantly influenced by the BMP signaling pathway. Modulating the level of CKS1B-K4 lactylation affects the interaction between CKS1B and cyclin-dependent kinase 1–3(CDK1–3), thereby altering CDK1–3 phosphorylation and activity, which is significant because CDK1–3 are critical regulators of cell cycle progression that drive transitions between different phases of the cell cycle. Additionally, changes in CKS1B-K4 lactylation influence the binding of CKS1B to p27, thereby affecting p27 phosphorylation and promoting its ubiquitination and degradation, which relieves the inhibitory effect of p27 on CDK activity and consequently facilitates cell cycle progression. Importantly, CKS1B-K4 lactylation is a critical mediator through which BMP9 promotes CDK1-3 phosphorylation and p27 ubiquitination. Furthermore, the BMP receptor inhibitor LDN-212854 was found to suppress CDK1-3 phosphorylation and p27 ubiquitination. Overall, our findings indicate that CKS1B-K4 lactylation, a novel post-translational modification, serves as a key molecular mechanism through which BMP9 drives cell cycle progression and promotes HCC progression. Targeting the BMP

signaling pathway or CKS1B-K4 lactylation holds promise as a potential therapeutic strategy for treating HCC.

Key Words: BMP9, HCC, Cell cycle progression, CKS1B, Lactylation

1.Introduction

Bone morphogenetic protein 9 (BMP9), an important member of the transforming growth factor β (TGF-β) superfamily, plays a critical role in the development and progression of hepatocellular carcinoma (HCC)[1]. Approximately 40% of HCC tissues exhibit elevated BMP9 expression, which correlates with poor prognosis[2]. BMP9 promotes HCC progression by regulating the cell cycle, cancer stemness, and the tumor microenvironment through downstream effectors such as Snail and ID1[3, 4]. Although BMP9 has been reported to influence HCC progression via post-translational modification of cell cycle-related molecules, the precise mechanisms remain unclear. Identifying key downstream targets of BMP9 in cell cycle regulation is therefore essential for understanding HCC pathogenesis and developing molecularly targeted therapies.

A hallmark of tumor metabolism is the heavy reliance on glycolysis, which generates large amounts of lactate—a phenomenon known as the Warburg Effect[5]. .Beyond serving as an energy source, lactate has recently been identified as a substrate for lactylation, a novel post-translational epigenetic modification first reported by Zhang et al. in 2019[6], occurring on lysine (K) residues and altering protein structure and function[7]. Analogous to other lysine acylation modifications, lactylation is regulated by "writers" such as p300 and CREB-binding protein (CBP), and "erasers" including Class I histone deacetylases (HDAC1–3) and Class III histone deacetylases (SIRT1–3)[8, 9].

Lactylation plays a significant role in HCC[10]. Lysine lactylation (Klac) is associated with HCC progression, poor prognosis, dysregulated liver-specific metabolic pathways, and downregulation of the p53 tumor suppressor pathway[11]. Site-specific lactylation events have been shown to drive HCC malignancy through diverse mechanisms: K76 lactylation of IGF2BP3 reinforces the IGF2BP3-PCK2-SAM-m6A loop to promote lenvatinib resistance[12]; K230/K322 lactylation of ALDOA facilitates DDX17 nuclear translocation to enhance HCC stemness, with H3K56 lactylation being one of the most prevalent sites in HCC stem cells[13]; K90 lactylation of YAP prevents its CRM1-mediated nuclear export, promoting nuclear accumulation and HCC malignancy[14]; and K430 lactylation of ABCF1 activates the HIF pathway to drive HCC progression[15].

Cyclin-dependent kinase regulatory subunit 1B (CKS1B), a small regulatory subunit of CDKs, primarily interacts with CDK1–3 to regulate the G1/S and G2/M transitions[16] and modulates SCF complex-mediated ubiquitination and degradation of substrates such as p27 (Kip1)[17]. Aberrant CKS1B expression has been implicated in HCC progression and poor prognosis, making it a promising therapeutic target[18, 19, 20]. In this study, we demonstrate that BMP9 promotes CKS1B lactylation—a novel post-translational modification—to regulate the cell cycle and drive HCC progression, thereby uncovering a key downstream pathway of BMP9 and underscoring the importance of lactylation in HCC biology.

2.Result

2.1 BMP9 promotes CKS1B-K4 lactylation in HCC

To investigate the correlation between BMP9 expression in HCC tissue specimens and patient prognosis, we analyzed BMP9 expression in tissue samples from 47 HCC patients using IHC staining. Patients with higher BMP9 expression in HCC tissue

compared to adjacent liver tissue were categorized as BMP9-high, while those with equal or lower BMP9 expression in HCC tissue were categorized as BMP9-low(Figure 1A). To further elucidate the prognostic significance of BMP9 expression in HCC patients, we divided these 47 patients into two groups based on the differential expression of BMP9 between tumor tissue and adjacent liver tissue and subsequently evaluated their overall survival. Interestingly, patients in BMP9-high group(n=21) exhibited significantly poorer overall survival compared to those in BMP9-low group(n=26)(p = 0.0004, Figure 1B, Cohort 1).

Next, we investigated the impact of BMP9 on the lactylation of proteins in HCC cell lines(Huh7 and Hep3B). We treated Huh7 and Hep3B cells with BMP9 or LDN-212854(inhibitor of BMP signaling pathway). As expected, the results showed that BMP9 significantly increased the pan-Klac levels in Huh7 and Hep3B cells(Figure 1C), while LDN-212854 significantly reduced the pan-Klac levels in these two cell lines(Figure 1D). The results of xenograft models also showed that LDN-212854 reduced the pan-Klac levels in tumor tissues(Figures 1E and F). These findings indicate that the BMP signaling pathway plays a critical role in regulating protein lactylation in HCC.

It is well known that an increase in intracellular lactate levels leads to elevated protein lactylation. Therefore, we measured lactate levels in HCC cells treated with BMP9 or LDN-212854. However, neither BMP9 nor LDN-212854 had a significant effect on intracellular lactate levels in HCC cells (Figure S1A), suggesting that the BMP signaling pathway regulates protein pan-Klac levels through a lactate-independent mechanism that requires further investigation. To systematically identify BMP signaling-dependent Klac modifications in HCC cells, we next sought to perform integrated proteomic and

lactylomic analyses. We chose LDN-212854 as the perturbation tool for several reasons. First, LDN-212854 is a highly selective small-molecule inhibitor of BMP type I receptors (ALK1/ALK2), enabling specific blockade of BMP signaling without the confounding off-target effects associated with ligand stimulation or genetic manipulation. Second, compared with exogenous BMP9 stimulation—which may be buffered by endogenous ligand–receptor dynamics and feedback regulation—pharmacological inhibition produces a more robust and reproducible suppression of pathway activity, thereby maximizing the dynamic range for detecting differentially lactylated proteins. Third, LDN-212854 exerted a strong suppressive effect on HCC cell proliferation and cell cycle progression in our preceding assays, indicating that the molecular alterations induced by this inhibitor are functionally linked to the BMP9-driven phenotypes of interest. Finally, using a loss-of-function approach allowed us to focus on lactylation events that are actively maintained by BMP signaling, which are more likely to represent direct, pathway-dependent regulatory nodes amenable to therapeutic targeting.

Accordingly, we performed proteomic and lactylomic analyses on Hep3B cells treated with LDN-212854 (Figure 1G). A total of 5563 proteins were identified (Figure S1B), among which 1029 were lactylated proteins, with 2141 lactylation sites detected in total (Figure S1C). Differential analysis revealed that 124 proteins were upregulated and 97 were downregulated, while 134 lactylation sites showed increased abundance and 117 showed decreased abundance (Figure S1D). Network-based gene ontology (GO) and functional enrichment analyses revealed that proteins with decreased lactylation were involved in key molecular processes such as RNA biosynthesis and cell cycle progression

(Figures 1H and 1I). Among the cell cycle-associated proteins with reduced lactylation, the affected sites included Cyclin-Dependent Kinase Regulatory Subunit 1B-Lysine 4 (CKS1B-K4), Cyclin-Dependent Kinase Regulatory Subunit 2 (CKS2-K4), DDB1 and CUL4 Associated Factor 1 (DCAF1-K284), Retinoblastoma-Like 1 (RBL1-K1015, also known as p107), and Cell Division Cycle 37 (CDC37-K126). Notably, CKS1B-K4 exhibited the most pronounced decrease in lactylation, with a fold change of −1.57 (Figure 1J and K), ranking among the top 30 sites with the largest reductions (Figure 1L). These findings prompted us to focus on the molecular mechanism by which BMP9 regulates cell cycle progression in HCC cells through CKS1B K4 lactylation.

2.2 Expression of CKS1B-K4 lactylation is closely associated with the prognosis of HCC patients

Having identified CKS1B-K4 as the most prominently affected lactylation site by BMP signaling, we next sought to validate its clinical relevance and functional significance in HCC. To investigate the effect of CKS1B-K4 lactylation in HCC, we performed IHC staining analysis of human HCC tissues using a custom lactylation site antibody targeting CKS1B-K4 lactylation. Similarly, HCC patients with CKS1B-K4 lactylation levels higher than those in adjacent liver tissues were classified into the CKS1B-K4lac-high group, and those with lactylation levels equal to or lower than those in adjacent tissues were classified into the CKS1B-K4lac-low group. IHC staining results showed that 15 patients were classified in CKS1B-K4lac-high group, and 32 were in CKS1B-K4lac-low group. The results showed that patients with high CKS1B-K4 lactylation expression (CKS1B-K4lac-high, n=15) had significantly worse overall survival compared to those

with low CKS1B-K4 lactylation expression (CKS1B-K4lac-low, n=32) (p=0.0336, Figure 2A). Also, we identified a significant association between BMP9 expression and the CKS1B-K4lac level (p=0.0014, Figure 2B and C). Additionally, clinical feature analysis of these patients showed that elevated CKS1B-K4 lactylation expression in HCC tissues was significantly associated with serum PIVKA-II levels and patterns of HCC recurrence (Table1). These findings indicate that the expression levels of BMP9 and CKS1B-K4 lactylation in tumor tissues are significantly correlated and that their elevated expression is associated with poorer overall survival, making them potential prognostic biomarkers for HCC.

Due to the current lack of methods to directly mimic lactylation modifications, we constructed mutant plasmid by mutating lysine at position 4 (K4) of CKS1B to arginine (K4R) to simulate the delactylation state at this site. CCK-8 assays and colony formation experiments showed that compared to Huh7 and Hep3B cells transfected with wild-type CKS1B plasmid (CKS1B-WT), cells transfected with the CKS1B-K4R mutant plasmid exhibited significantly reduced proliferation (Figure 2D and E). Flow cytometry analysis further revealed that the cell cycle progression of Huh7 and Hep3B cells transfected with the CKS1B-K4R mutant plasmid was significantly delayed compared to those transfected with the CKS1B-WT plasmid (Figure 2F). Subsequently, we used a lentivirus system to establish Hep3B cell lines stably expressing CKS1B-WT and CKS1B-K4R, respectively, and developed a mouse subcutaneous xenograft tumor model based on these two stable cell lines. The results showed that xenograft tumors formed by Hep3B-CKS1B-K4R cells were significantly smaller in both volume and weight compared to those formed by Hep3B-CKS1B-WT cells (Figures 2G, H, and I). In summary, these results shows that CKS1B-K4 lactylation plays pivotal role in cell cycle progression of HCC, further mechanism is worth in-depth study.

2.3 BMP9 promotes cell cycle progression in HCC and regulates the expression of cell cycle-related proteins

Having established that CKS1B-K4 lactylation is functionally important for HCC progression, we next examined the broader effect of BMP9 on cell cycle progression and sought to identify the downstream effectors connecting CKS1B to the cell cycle machinery. CCK-8 and colony formation assays showed that BMP9 significantly promoted proliferation of HCC cells, whereas the BMP receptor inhibitor LDN-212854 markedly suppressed proliferation in Huh7 and Hep3B cells (Figure 3A-D). In addition, LDN-212854 significantly inhibited Hep3B-derived tumor growth in a mouse xenograft model (Figure 3E, F, and S2A, S2B). Flow cytometry further revealed that BMP9 decreased the proportion of cells in G1 phase and increased that in S phase, while LDN-212854 blocked the G1/S transition (Figure 3G and H).

Next, we queried the STRING database (https://string-db.org/) (Figure S2C and D) and HitPredict (https://www.hitpredict.org/index.html) (Figure S2E) to identify proteins showing the strongest interactions with CKS1B. Based on the results from these databases and the known functions of these proteins, we selected the following candidates for further study: CDK1-3, the direct drivers of cell cycle progression that phosphorylate p27 at Thr187 to prime it for degradation; CDKN1B (p27), a tumor suppressor that inhibits CDK–cyclin activity and thereby restrains cell cycle progression; and SKP2, the substrate-recognition component of the SCF^SKP2 E3 ubiquitin ligase complex that, together with CKS1B as an essential cofactor, recognizes phosphorylated p27 and targets it for ubiquitination and proteasomal degradation. These candidates collectively cover the two opposing arms of cell cycle regulation converging on CKS1B: the cell-cycle-promoting arm (CDK1–3 and the SKP2–CKS1B-mediated degradation of p27) and the cell-cycle-inhibiting arm (p27-mediated suppression of CDK activity). This

selection therefore allows us to systematically evaluate how CKS1B-K4 lactylation influences both the positive and negative regulatory circuits governing cell cycle progression. Western blot analysis showed that BMP9 increased the expression of CDK1-3, CKS1B, and SKP2, while decreasing p27 expression (Figure 3I). In contrast, LDN-212854 reduced CDK1-3, CKS1B, and SKP2 expression and increased p27 levels in both HCC cells and xenograft tumors (Figure 3J and K). Collectively, these findings suggest that BMP9 plays a role in regulating the cell cycle progression of HCC.

2.4 CKS1B-K4 lactylation influences the interaction between CKS1B and CDK1-3, as well as the phosphorylation of CDK1-3

To further investigate the mechanism how CKS1B-K4 lactylation influences HCC cell cycle progression, we transfected Hep3B and Huh7 cells with the wild-type CKS1B-WT plasmid and the mutant CKS1B-K4R plasmid to observe the effect of changes in CKS1B-K4 lactylation levels on the interaction between CKS1B and CDK1-3. Co-immunoprecipitation (Co-IP) experiments demonstrated that reducing CKS1B-K4 lactylation significantly inhibited the direct interaction of CKS1B with CDK1-3(Figure 4A and B).

CKS1B facilitates the phosphorylation of CDK1 at threonine 161 (T161) and CDK2/3 at threonine 160 (T160), which is essential for activating their kinase activity[20, 21]. Based on this, we attempted to explore how CKS1B-K4lac influences the phosphorylation modifications of CDK1-3. We found that the reduction of CKS1B-K4 lactylation markedly suppressed the phosphorylation of threonine 161 (T161) of CDK1 and threonine 160 (T160) of CDK2/3 (Figure 4C). These findings indicate that CKS1B-K4 lactylation is a key factor regulating the proliferation of HCC cells. Its mechanism is primarily achieved by

influencing the interaction between CKS1B and CDK1-3, as well as the phosphorylation of CDK1-3.

2.5 BMP9 promotes CKS1B-K4 lactylation levels and the interaction between CKS1B and CDK1-3

To investigate the effects of BMP signaling pathway activity on CKS1B-K4 lactylation level and its interaction with CDK1-3, we treated Huh7 and Hep3B cells with BMP9 or LDN-212854 for 48 hours. Co-IP using anti-CKS1B antibodies followed by immunoblotting with anti-CDK1-3 and anti-Pan-Klac antibodies confirmed the BMP9 significantly increased CKS1B-K4 lactylation level, while also enhancing the interaction between CKS1B and CDK1-3 (Figure 5A). This interaction was further confirmed through reverse immunoprecipitation using anti-CDK1, CDK2 and CDK3 antibodies and subsequent immunoblotting with anti-CKS1B antibodies (Figure 5B). Furthermore, Co-immunoprecipitation analysis revealed that, in contrast, LDN-212854 significantly decreased CKS1B-K4 lactylation and suppressed the interaction between CKS1B and CDK1–3. (Figure 5C and D).

2.6 BMP9 increases HCC cell cycle progression and the interaction between CKS1B and CDK1-3 though CKS1B-K4 lactylation

To investigate whether BMP9 regulates the cell cycle progression of HCC cells through CKS1B-K4 lactylation modification, we treated Huh7 and Hep3B cells transfected with CKS1B-WT and CKS1B-K4R plasmids with BMP9. Results from the CCK-8 assay and colony formation experiments showed that BMP9 significantly promoted the proliferation of Huh7 and Hep3B cells. Nevertheless, delactylation of CKS1B-K4 (K4R mutation)

significantly weakened the proliferative effect of BMP9 on HCC cells (Figures 6A and B). Flow cytometry analysis further revealed that BMP9 accelerated the cell cycle progression of Huh7 and Hep3B cells, whereas reduced CKS1B-K4 lactylation (K4R mutation) significantly inhibited the ability of BMP9 to promote cell cycle progression in these cells (Figure 6C). Moreover, Co-IP results showed that BMP9 significantly increased CKS1B-K4 lactylation level and enhanced the interaction between CKS1B and CDK1-3. However, reduced CKS1B-K4 lactylation (K4R mutation) markedly impaired the ability of BMP9 to enhance the interaction between CKS1B and CDK1-3 (Figures 6D and 6E). Additionally, BMP9 significantly promoted the phosphorylation of CDK1-T161 and CDK2/3-T160 under WT-CKS1B expression, while the phosphorylation of CDK1-T161 and CDK2/3-T160 were markedly suppressed under the delactylation of CKS1B-K4 (K4R mutation) expression (Figure 6F). These findings indicate that CKS1B-K4 lactylation is the key molecular mechanism by which BMP9 regulates the interaction between CKS1B and CDK1-3 and promotes the phosphorylation of CDK1-T161 and CDK2/3-T160.

2.7 BMP9 promotes the interaction between CKS1B and p27 and enhances p27 ubiquitination through CKS1B-K4 lactylation

In addition to directly cooperating with CDK1-3 to drive cell cycle progression, CKS1B also facilitates SCF-SKP2 mediated recognition and ubiquitination of p27, a major CDK inhibitor. Thus, CKS1B functionally links CDK activation with p27 turnover during cell cycle progression. Based on this, we next focused on p27 as a potential downstream target of BMP9/CKS1B signaling. p27 is a critical regulator of the cell cycle and a key tumor suppressor. We showed that BMP9 decreased the expression of p27, whereas treatment with LDN-212854 increased its expression. The result showed that BMP9 decreased the

expression of p27, whereas treatment with LDN-212854 increased its expression. We next investigated the mechanism by which BMP9 regulates the ubiquitination of p27. We analyzed the expression levels of p27 in Huh7 and Hep3B cells transfected with CKS1B-WT and CKS1B-K4R plasmids. Western blot results showed that wild-type CKS1B (CKS1B-WT) reduced p27 expression levels, whereas the K4R mutant, which exhibits reduced lactylation, partially restored p27 expression (Figure 7A). It was reported that p27 phosphorylation is closely linked to ubiquitination and subsequent degradation. Specifically, phosphorylation at Serine 10 (S10) and Threonine 187 (T187) promotes its ubiquitination and degradation, while phosphorylation at Threonine 198 (T198) inhibits these processes. Subsequently, we treated Huh7 and Hep3B cells transfected with CKS1B-WT and CKS1B-K4R plasmids with MG132 (a commonly used proteasome inhibitor) to further investigate the effects of CKS1B-K4 lactylation on p27 phosphorylation levels. Western blot analysis revealed that reduced CKS1B-K4 lactylation (K4R mutation) significantly suppressed the phosphorylation of p27 at S10 and T187 while enhancing phosphorylation at T198 (Figure 7B). BMP9 promotes the phosphorylation of p27 at S10 and T187 while suppressing its phosphorylation at T198. In contrast, reduced CKS1B-K4 lactylation (CKS1B-K4R mutant) significantly inhibits BMP9-induced phosphorylation of p27 at S10 and T187 and attenuates the suppressive effect of BMP9 on T198 phosphorylation (Figure 7C). We further investigated whether BMP9 regulates the interaction between CKS1B and p27 and the ubiquitination of p27 through CKS1B-K4 lactylation. Co-IP results showed that BMP9 significantly enhanced the interaction between CKS1B and p27 and increased p27 ubiquitination (Figure 7D). In contrast, the BMP receptor inhibitor LDN-212854 suppressed the interaction between CKS1B and p27 and reduced p27 ubiquitination (Figure 7E). Additionally, reduced CKS1B-K4 lactylation (CKS1B-K4R mutant) significantly inhibited the interaction between CKS1B and p27 and

the ubiquitination of p27 (Figure 7F). Further studies demonstrated that reduced CKS1B-K4 lactylation markedly suppressed the interaction between CKS1B and p27 and the ubiquitination of p27 induced by BMP9 (Figure 7G). In conclusion, these findings indicate that BMP9 promotes the interaction between CKS1B and p27 and enhances p27 ubiquitination by regulating CKS1B-K4 lactylation, thereby facilitating p27 degradation via the lysosomal pathway and contributing to cell cycle progression .

2.8 CKS1B-K4 lactylation modifies the docking conformation of CKS1B in its interactions with CDK1-3 and p27, while also reducing the molecular binding energy

To further explore the effect of K4 lactylation on CKS1B, molecular dynamics (MD) simulations were performed on CKS1B-K4lac. First, the full sequence of CKS1B (P61024) was obtained from the UniProt website (https://www.uniprot.org/), and its molecular structure was predicted using the AlphaFold Server (https://alphafoldserver.com/). After manually adding a lactyl group to K4, MD simulations were conducted using GROMACS. The results showed that the K4 lactylation did not cause significant changes to the molecular structure of CKS1B (Figure S3A and B). Subsequently, protein-protein docking was performed using MOE to analyze the interactions between CDK1-3, p27 with both CKS1B-WT and CKS1B-K4lac. The docking results showed that although K4 and K4lac residues did not participate directly in the interaction between the two proteins, K4lac influenced the docking pose of CKS1B with CDK1-3 and p27, and reduced the docking binding energy (Figure 8A-D, Table 2). These results align with the Co-IP experimental findings, which demonstrate that K4 lactylation enhances the interaction between CKS1B and CDK1-3, as well as p27.

2.9 p300 is the writer of CKS1B-K4 lactylation, and BMP9 promotes p300 expression via pSmad1/5

Currently, p300 and CBP are the only known writers of lactylation modifications[22]. To identify the specific writer responsible for CKS1B-K4 lactylation, we constructed Flag-p300 and Flag-CBP tagged protein plasmids and transfected them into Huh7 and Hep3B cells. Co-IP results showed that p300 is the primary writer of CKS1B lactylation (Figure 9A). To further validate the role of p300 in CKS1B lactylation, we transfected siRNA targeting p300 into Huh7 and Hep3B cells to knock down its expression. Co-IP results indicated that knocking down p300 significantly reduced the pan-Klac level of CKS1B (Figure 9B). Furthermore, BMP9 significantly enhanced the pan-Klac of CKS1B, but knocking down p300 suppressed this BMP9-induced enhancement of CKS1B lactylation (Figure 9C). These findings suggest that BMP9 promotes CKS1B lactylation through the upregulation of p300 expression.

BMP9 regulates the expression of downstream target proteins primarily through the BMP-specific R-Smad (BR-Smad) pathway, which is activated by the phosphorylation of pSmad1/5/8. The BMP9-induced phosphorylated Smad1/5/8 complex enters the nucleus and binds to the promoters of target genes, promoting their mRNA expression[2, 23]. Our qPCR and Western blot results demonstrated that BMP9 significantly increased p300 mRNA and protein expression levels in Huh7 and Hep3B cells, whereas the BMP receptor inhibitor LDN-212854 suppressed this effect (Figures 9D and E). Additionally, BMP9 increased pSmad1/5 levels, while LDN-212854 reduced pSmad1/5 levels (Figures 9D and E). Previous studies have shown that BR-Smad (Smad1/5/8) preferentially binds to GC-rich motifs, known as GC-SBE (GC-Rich Smad Binding Elements), whose core

sequence is GGCGCC. This palindromic sequence structure enhances BR-Smad binding affinity. These binding motifs are widely present in the promoters of BMP target genes[24]. Non-palindromic variants, such as GGCTCC, GGAGCC, and GGTGCC, also exist (Figure 9F)[25, 26]. In different cell types, BR-Smad can bind with specific cofactors to selectively recognize different motifs. For example, in human umbilical vein endothelial cells (HUVECs), 69.7% of GGCTCC binding sites lose BMP sensitivity under fluid shear stress[25]. We identified eight GC-SBE motifs in the p300 promoter (Figure 9G, Figure S4). To explore which motif pSmad1/5 binds to induce p300 transcription, we first constructed a luciferase reporter gene vector containing the full-length p300 promoter and transfected it into Huh7 cells. After 48 hours of BMP9 treatment, luciferase assays showed that BMP9 increased the transcriptional activity of the p300 promoter (Figure 9H). Next, we truncated the p300 promoter at position -989 and constructed two truncated luciferase reporter vectors, spanning -2100→-989 and -989→0, respectively, and transfected them into Huh7 cells. Luciferase assays indicated that the transcriptional activity of the -2100→-989 fragment was the highest, while the -989→0 fragment had activity comparable to the full-length promoter (Figure 9I). This suggests that the most active transcriptional region of the p300 promoter lies within the -2100→-989 segment. The higher activity of the truncated promoter fragment than that of the full-length promoter also suggests that upstream or downstream regions outside this segment may contain repressive cis-regulatory elements that attenuate p300 transcription. Notably, BMP9 treatment significantly increased the transcriptional activity of this region in Huh7 cells, whereas the activity of the -989→0 fragment remained unchanged (Figure 9J). These findings indicate that BMP9 specifically enhances the transcriptional activity of the -2100→-989 region. We further constructed shorter truncated vectors within the -2100→-989 region to identify

which GC-SBE motifs are critical for p300 promoter activity (Figure 9K). Luciferase assays revealed that the -2100→-989 segment exhibited the highest transcriptional activity, whereas the -2100→-1115 segment demonstrated reduced activity. Notably, the -2100→-1257 fragment completely lost transcriptional activity (Figure 9L). Additionally, BMP9 treatment of Huh7 cells significantly enhanced the transcriptional activity of the -2100→-989 fragment, but showed no stimulatory effect on the -2100→-1115 segment (Figure 9M). This further confirms that BMP9 promotes p300 expression by increasing the transcriptional activity of the -1115→-989 region.

To investigate whether BMP9 regulates the -2100→-989 region of the p300 promoter through p-Smad1/5, we used Smad1-specific siRNA to knock down Smad1 expression in Huh7 cells, which effectively reduced pSmad1/5 levels (Figure 9N). Luciferase assays demonstrated that BMP9 significantly enhanced the transcriptional activity of the -2100→-989 region of the p300 promoter, and this effect was abolished when Smad1 was knocked down (Figure 9O). Within the -1115→-989 region, mutating the GC-SBE motif at -1072 (GGCTCC) to GATCTC completely abolished BMP9-induced transcriptional activity, while the wild-type -1115→-989 fragment maintained BMP9 responsiveness (Figure 9P and Q). Furthermore, Chromatin Immunoprecipitation-PCR (ChIP-PCR) results showed that BMP9 promotes pSmad1/5 binding to the GC-SBE motif (GGCTCC) at -1072 in the p300 promoter (Figure 9R). Collectively, these findings indicate that BMP9 enhances p300 transcription by upregulating pSmad1/5 levels and promoting its binding to the GC-SBE motif at -1072 in the p300 promoter.

3.Discussion

BMP9 is closely linked to the development and progression of HCC. Our previous study reveals that BMP9 plays a pivotal role in regulating cell cycle progression in HCC. The regulation of cell cycle progression is a fundamental mechanism driving tumorigenesis and cancer progression, making it a critical target for the prevention and treatment of HCC. Although cell cycle-targeting drugs, such as cyclin-dependent kinase 4/6 (CDK4/6) inhibitors, have been widely used in cancer therapy, they are often associated with significant side effects[27]. For instance, abemaciclib, used in treating advanced breast cancer, can lead to rare but severe pulmonary inflammation[28]. Therefore, the development of highly effective anticancer drugs with low side effects remains an urgent need in cancer research. In the treatment of HCC, an ideal therapeutic target should be highly expressed in HCC cells while being minimally expressed or absent in normal cells. By knocking out or inhibiting such targets, it would be possible to significantly suppress the proliferation of HCC cells while minimizing effects on normal cells, thereby improving the safety and efficacy of treatment. our data showed that BMP9 expression levels higher in HCC patients than those in adjacent liver tissues and the elevated expression is associated with poorer overall survival, making it potential prognostic biomarkers for HCC (Figure 3 and table1).

The orderly progression of the cell cycle relies on the activation or inactivation of CDKs at specific times. CDKs, members of the serine/threonine protein kinase family, require the following three conditions for activation: (1) phosphorylation at activating sites and dephosphorylation at inhibitory sites; (2) no binding to cyclin-dependent kinase inhibitors (CKIs) such as p27; (3) binding to Cyclins. Phosphorylation at threonine 161(T161) of CDK1 and threonine 160(T160) of CDK2/3 activates their activity, while phosphorylation at threonine 14(T14) and tyrosine 15(Y15) of CDK1-3 inhibits them. CKS form the third subunit of the Cyclin-CDK complex and are highly conserved from yeast to mammals[17]. The mammalian genome encodes two CKS proteins (CKS1 and CKS2)[18],

among which CKS1 (namely CKS1B) is a key factor driving cell cycle progression[19]. CKS1B primarily regulates the phosphorylation of CDK1-3 at different sites by interacting with them[20, 21], thereby activating Cyclin-CDK complexes such as CyclinB-CDK1, CyclinA-CDK2, and CyclinC-CDK3 to promote cell cycle progression. Given the role of CKS1B in Cyclin-CDK regulation，our study revealed that BMP9 promotes CKS1B-K4 lactylation, which enhances the interaction between CKS1B and CDK1-3. This, in turn, promotes the phosphorylation of CDK1-T161 and CDK2/3-T160, thereby accelerating the cell cycle progression of HCC cells (Figure 11). CKS1B is considered a critical factor in promoting tumorigenesis and disease progression in HCC. It promotes the degradation of cell cycle inhibitors such as P21WAF1(p21), P27KIP1(p27), P57KIP2(p57), p130, RASSF1A, and FOXO1, weakening tumor-suppressive signals and enhancing cancer cell survival[18]. In line with the report, we found that BMP9 promotes the interaction between CKS1B and p27 and enhances p27 ubiquitination through CKS1B-K4 lactylation, thereby facilitating p27 degradation.

p27, encoded by the CDKN1B gene, is a well-established tumor suppressor whose function is tightly regulated by various post-translational modifications[29]. It primarily functions by binding to CyclinE-CDK2 or CyclinD-CDK4 complexes to inhibit their activation, thereby arresting the cell cycle at the G1 phase. The phosphorylation status of p27 is tightly linked to its ubiquitination and stability. Phosphorylation at S10 and T187 facilitates p27 ubiquitination and subsequent degradation, whereas phosphorylation at T198 stabilizes p27 by inhibiting its ubiquitination and degradation[30]. phospho-p27(T187) could be specifically recognized by SKP2, which is an essential component of the SCF (Skp1-Cullin1-F-box) E3 ubiquitin ligase complex. Phospho-p27(T187) recognition by SKP2 is crucial for its binding to the SCF-SKP2 complex[31]. Once bound, the SCF-SKP2 complex—composed of SKP2 (substrate recognition), Skp1, Cullin1 (Cul1) and Rbx1,

facilitates the polyubiquitination of p27. CKS1B not only promotes cell cycle progression by binding to CDK1-3 but also participates in forming the ubiquitin ligase SKP2-CKS1B complex, which facilitates p27 ubiquitination and degradation[32]. This degradation reduces CDK-p27 binding, relieving the inhibition of CDK activity and enabling a smooth transition of the cell cycle from G1 to S phase, providing the necessary conditions for subsequent cell division[33, 34]. Our data reveal that BMP9 induces SKP2 expression and promotes p27 phosphorylation at S10 and T187, while inhibiting its phosphorylation at T198 through CKS1B-K4 lactylation. Collectively, these mechanisms drive a reduction in the protein level of p27.

Notably, beyond promoting p27 ubiquitination and degradation, CKS1B mediates IL-8 expression via the NF-κB pathway, contributing to hepatocarcinogenesis[35]. Additionally, CKS1B regulates the JAK/STAT3 signaling pathway by activating pSTAT3 protein expression and modulating downstream target genes such as TIMP-1, Bcl-2, and VEGF, further driving HCC progression[36]. Moreover, it influences DUSP16 expression through activation of the ERK1/2 signaling pathway, leading to upregulation of osteopontin (OPN), which also promotes HCC progression[37]. These findings suggest that CKS1B can also exert tumor-promoting effects in HCC independently of Skp2. Furthermore, CKS1B may also be involved in regulating multidrug resistance in HCC, enhancing the tolerance of HCC cells to chemotherapy or targeted therapies[38]. Given its multifaceted tumor-promoting roles, CKS1B is considered an ideal therapeutic target, and inhibiting its expression or function could be a promising strategy for future HCC treatment.

However, as an intrinsically disordered protein, CKS1B lacks well-defined small molecule binding pockets suitable for drug development. Nevertheless, studies have shown that the pocket structure formed by the SKP2-CKS1B-p27 interaction could serve as a potential target for small molecule inhibitors[18]. Research on whether druggable pockets

exist in complexes formed by CKS1B and other proteins remains limited. In future studies, we aim to investigate potential druggable pockets within the complexes formed by CKS1B-WT/K4lac and CDK1-3 or p27. Additionally, we will establish a virtual small molecule compound library, screen for lead compounds, and further optimize their design for drug development to target those complexes. This research holds great potential for application and provides new possibilities for developing small molecule inhibitors targeting the CKS1B complex.

Protein lactylation is a covalent modification occurring on lysine residues, where a lactyl group ($C_3H_4O_3$) is chemically acylated to the ε-amino group of lysine. This process is catalyzed by p300 and CBP, which are histone acetyltransferases (HATs). These two HAT enzymes are among the most extensively studied 'writers' involved in lactylation modification. Recent research has identified several target proteins that undergo lactylation through the activity of p300 and CBP: p300 has been shown to catalyze the lactylation of proteins such as Yin Yang-1(YY1)-K183, MeCP2-K210/K249, Nucleolin(NCL)-K477, and ARRB1[39, 40, 41, 42], while CBP has been identified as the lactyltransferase for proteins like Targeting Protein for Xklp2 (TPX2) and meiotic recombination 11(MRE11)-K673[43, 44]. Both p300 and CBP are capable of lactylating proteins such as Twist1-K150, Snail, and H3K18[45, 46, 47]. In addition to p300 and CBP, recent studies have reported that alanyl-tRNA synthetase 1 (AARS1) and AARS2 also possess lactyltransferase activity[48, 49], with AARS1 promoting the lactylation of YAP[50], and AARS2 catalyzing the lactylation of p53[51]. Furthermore, studies have shown that certain members of other HAT families also exhibit lysine lactyltransferase activity, such as GNAT13 from the GNAT family, which has been demonstrated to possess lysine lactyltransferase activity[52]. Whether other members of the HAT family also have lysine lactyltransferase activity remains to be further investigated. Our study identified p300 as the writer responsible for the lactylation

of CKS1B, and p300 is upregulated by BMP9. BMP9 enhances p300 transcription by increasing the expression of pSmad1/5, which facilitates the binding of these phosphorylated Smad proteins to the GC-SBE (GGCTCC) motif located in the -1072 region of the p300 promoter. This lactylation mechanism underscores the critical role of BMP9 in driving cell cycle progression in HCC cells through p300-mediated CKS1B lactylation.

Our study is the first to identify CKS1B(CKS1B-K4) as a novel site of lactylation, which is closely associated with cell cycle regulation in HCC cells. Furthermore, we elucidated the mechanism by which BMP9 regulates CKS1B-K4 lactylation via the histone acetyltransferase p300. Our research provides a highly innovative and groundbreaking contribution to the field, offering new insights and potential molecular targets for the investigation and treatment of HCC.

4. Materials and Methods

4.1 Clinical samples

A total of 47 resected HCC tissue specimens (from cohorts 1 and 2) were collected with informed consent from patients who underwent liver resection at Western China Hospital of Sichuan University between 2018 and 2019. All participants provided written informed consent, agreeing to the use of their tissue samples for future research. The study was conducted in compliance with the Declaration of Helsinki, and the research protocols were approved by the Ethics Committee of Western China Hospital of Sichuan University (Approval No. 2016-91).

4.2 Animal Studies

NOD/ShiLtJGpt-*Prkdc*^{em26Cd52}*Il2rg*^{em26Cd22}/Gpt Coisogenic Genetically Engineered Immunodeficient mice (NCG mice) were purchased from GemPharmatech Co., Ltd. (Nanjing, China) and maintained under specific pathogen-free conditions with a 12-hour light/dark cycle. The mice were provided with unrestricted access to tap water and standard chow. HCC cells (1×10^6) were resuspended in 200 μL of a 1:1 mixture of DMEM and Matrigel (Corning, BD Biosciences, Franklin Lakes, New Jersey, USA) and subcutaneously injected into NCG mice aged 4 to 6 weeks. Once the tumors reached a measurable size, the mice were randomly divided into two groups (n=5 per group) for LDN-212854 treatment. Mice were intraperitoneally administered either PBS or 6 mg/kg of LDN-212854 twice daily for 10–14 days. Tumor dimensions were recorded twice weekly. All animal experiments were conducted in accordance with the principles of laboratory animal care (NIH publication no. 85-23, revised 1985). The experimental protocol was approved by the Sichuan University Animal Care and Use Committee and adhered to the Guide for the Care and Use of Laboratory Animals prepared by the National Academy of Sciences.

4.3 Cell lines and Reagents

The HCC cell lines Huh7 and Hep3B were purchased from Procell Life Science & Technology Co., Ltd. (Wuhan, China). The cells were cultured in Dulbecco's Modified Eagle Medium (DMEM; Gibco, Grand Island, NY, USA) supplemented with 10% fetal bovine serum (FBS; Gibco) and maintained at 37 °C in a humidified atmosphere with 5% CO_2.

4.4 RNA Interference and Plasmid Transfection

SiRNA and negative control siRNA were purchased from RIBOBIO (Guangzhou, China). Cells were cultured in medium without fetal bovine serum (FBS) for 24 hours prior to siRNA transfection. SiRNA constructs were transfected using Lipofectamine RNAiMAX (Invitrogen) following the manufacturer's instructions. Four to six hours post-transfection, cells were washed with PBS to completely remove residual siRNA constructs from the medium and were then cultured in DMEM supplemented with 10% FBS. The plasmid PCMV6-AC-GFP-ID1 (RG202061), as well as CKS1B-WT, CKS1B-K4R, Flag-p300, Flag-CBP, and the Luciferase Reporter Plasmid, were purchased from PAIVIBIO (Wuhan, China). The pcDNA3.1 (V790-20) plasmid, used as an empty vector control, was obtained from Invitrogen. DNA constructs were transfected using Lipofectamine 3000 (Invitrogen) according to the manufacturer's protocol. For co-transfection of siRNA and plasmids, Lipofectamine 2000 (Invitrogen) was used following the manufacturer's instructions. Similar to siRNA transfection, cells were washed with PBS 4–6 hours post-transfection to remove residual DNA constructs from the medium and were subsequently cultured in DMEM with 10% FBS.

4.5 Detection of Intracellular Lactate Concentration

HCC cells were suspended in PBS to prepare a cell suspension. The suspension was then subjected to ultrasonic lysis, and the lysate was mixed with the working solutions according to the instructions provided with the reagent kit (Lactic Acid Assay Kit, A019-2-1, Nanjing Jiancheng Bioengineering Institute). The mixture was incubated at 37℃ for 10 minutes, and the absorbance was measured at 530 nm using a microplate reader. The

intracellular lactate concentration was calculated by comparing the absorbance to a standard curve. The same lysate was used to determine the protein concentration, and the lactate concentration was normalized relative to the protein concentration.

4.6 Cell Proliferation Assay and Colony Formation

Cell proliferation was assessed using the Cell Counting Kit-8 (CCK-8, BIMAKE). A total of 2×10^3 cells were seeded into each well of a 96-well plate, with three replicates per condition. The cells were incubated at 37 °C for 1 hour, and absorbance at 450 nm was measured daily for three consecutive days using a microplate reader. For the colony formation assay, 2×10^3 treated cells were seeded into 6-well plates, with three replicates per condition. After 14 days of incubation, the plates were washed twice with phosphate-buffered saline (PBS), fixed with 4% formaldehyde for 10 minutes, and stained with 0.1% crystal violet solution (Cat#G1064, Solarbio) for 10 minutes. Colonies were then analyzed for further evaluation.

4.7 Cell Cycle Analysis

The cells were harvested and fixed with chilled 70% ethanol at 4 °C overnight. After discarding the ethanol, the cells were washed twice with PBS and resuspended in 250 μL of DNA staining solution (YEASEN Biotechnology, China) at room temperature for 30 minutes. Cell cycle analysis was performed using a CytoFLEX Flow Cytometer (Beckman Coulter, USA), and the resulting data were analyzed with FlowJo software.

4.8 Real-Time Quantitative PCR

Total RNA was isolated using the TRIzol reagent (Invitrogen, Carlsbad, CA, USA) and subsequently used for cDNA synthesis with the PrimeScript™ RT reagent kit (Takara, Japan). miRNA was extracted and purified using the miRNeasy® Mini Kit (Qiagen, Hilden, Germany) following the manufacturer's instructions. Quantitative PCR primers for ACTB and p300 were synthesized by Tsingke Biotechnology (Beijing, China), with all primer sequences provided in Table S4. Gene expression analysis was performed in triplicate using the LightCycler® 96 system (Roche, Rotkreuz, Switzerland), and relative fold changes were calculated using the 2^−ΔΔCT method.

4.9 Western blotting and Co-IP

Cell lysates were prepared using RIPA buffer (Cell Signaling Technology). For co-immunoprecipitation (Co-IP), 20 μg of protein lysate was used as input, while 1 mg of protein lysate was incubated with 30 μL of pre-washed A/G magnetic beads for 20 minutes at room temperature with rotation. The beads were then separated from the lysate using magnetic separation, and the pre-cleared lysate was transferred to clean tubes. Subsequently, the pre-cleared lysate (1 mg) was incubated with the primary antibody and an additional 30 μL of pre-washed A/G magnetic beads overnight at 4 °C. The immune complexes were washed with cold lysis buffer and eluted using sodium dodecyl sulfate (SDS) loading buffer. The eluted proteins were separated by SDS-polyacrylamide gel electrophoresis (SDS-PAGE) and transferred onto polyvinylidene fluoride (PVDF) membranes. The membranes were blocked with 5% skim milk for 1 hour at room temperature, followed by incubation with the primary antibody (overnight at 4 °C) and the secondary antibody (1 hour at room temperature). Protein expression was quantified using ImageJ v1.46 (National Institutes of Health, USA) and normalized to β-actin. For detecting

protein expression in Western blotting (WB) and immunoprecipitation, all antibodies were used at a 1:1000 dilution. Details of the antibodies and reagents used in this study are provided in Supplementary Information, Table S5.

4.10 Chromatin Immunoprecipitation assay

The Chromatin Immunoprecipitation (ChIP) assay was conducted using a ChIP kit (Catalog No. BK0045-01, ACE Biotechnology, Changzhou) according to the manufacturer's instructions. Cells were crosslinked with 1% formaldehyde for 10 minutes at room temperature, and the reaction was quenched with glycine solution (final concentration: 125 mM) for 5 minutes. After washing with pre-chilled PBS, the cells were lysed and sonicated in ChIP Sonication Buffer containing protease inhibitors to shear chromatin into fragments ranging from 200 to 1000 bp. The lysate was centrifuged at 12,000 rpm for 10 minutes at 4°C, and the supernatant containing chromatin was collected. For immunoprecipitation, 10–20 μg of chromatin was incubated with 2–5 μg of ChIP-grade primary antibody or IgG (negative control) at 4°C overnight. This was followed by incubation with equilibrated rProtein A/G MagPoly Beads for 1 hour at 4°C. The beads were sequentially washed with High Salt and Lysis Buffer, Low Salt Buffer, and TE Buffer. Chromatin was then eluted using ChIP Buffer containing Proteinase K and RNase, and crosslinks were reversed by incubating the mixture at 65°C for 4 hours. Finally, DNA was purified using spin columns as per the kit protocol and quantified by qPCR with target-specific primers.

4.11 IHC Staining

The primary antibodies used for immunohistochemistry (IHC) staining were the same as those used for Western blotting, as described above. IHC staining images were captured

using an Olympus BX63 microscope.

4.12 Dual-Luciferase Reporter Assay

Reporter gene vectors containing the p300 promoter (wild-type, truncated, and mutant versions) were individually cloned into the pmirGLO luciferase reporter vector (Promega, USA), which includes firefly luciferase (Luc2) as the reporter and Renilla luciferase (RLuc) as the internal control. The plasmids were transfected into HCC cells using Lipofectamine 3000, or co-transfected with siRNA using Lipofectamine 2000, depending on the experimental setup. Following transfection, cells were treated with BMP9 for 48 hours as required by the experiment. After 48 hours, cell lysates were collected, and luciferase activity was measured using the Dual-Luciferase Reporter Assay System (Promega) following the manufacturer's instructions.

4.13 Proteomic Analysis of Protein Post-translational Modifications Using LC-MS/MS and DIA Workflow

Samples were sonicated on ice for 3 minutes in lysis buffer (8 M urea, 1% protease inhibitor cocktail, 3 μM TSA, 50 mM NAM) and centrifuged at 12,000×g for 10 minutes at 4 °C to remove debris. The supernatant was collected, and protein concentrations were determined using a BCA assay kit. Proteins were precipitated with 20% TCA, incubated at 4 °C for 2 hours, and centrifuged at 4,500 × g for 5 minutes. The resulting pellets were washed with cold acetone, air-dried, and dissolved in 200

mM TEAB. Proteins were digested with trypsin at a 1:50 enzyme-to-protein ratio overnight at 37 °C. Reduction and alkylation were performed with 5 mM DTT (for 1 hour at 37 °C) and 11 mM IAA (for 45 minutes at room temperature in the dark). Peptides were desalted using Strata X SPE columns. The desalted peptides, dissolved in NETN buffer (100 mM NaCl, 1 mM EDTA, 50 mM Tris-HCl, 0.5% NP-40, pH 8.0), were incubated overnight with antibody-conjugated beads at 4 °C. Beads were washed sequentially with NETN buffer and water, and bound peptides were eluted with 0.1% trifluoroacetic acid. The eluted peptides were combined, vacuum-dried, and further desalted using C18 ZipTips. Peptides were dissolved in solvent A (0.1% formic acid, 2% acetonitrile in water) and separated on a homemade reversed-phase analytical column using a NanoElute UHPLC system (Bruker Daltonics) at a flow rate of 450–500 nL/min. The separated peptides were analyzed on a timsTOF Pro 2 mass spectrometer in dia-PASEF mode. Full MS scans were acquired over a range of 300–1700 m/z, and MS/MS scans were performed using optimized isolation windows and gradients. The DIA data were analyzed using Spectronaut software against the Homo_sapiens_9606_SP_20230103.fasta database, allowing for 2–4 missed cleavages. Carbamidomethylation of cysteine was set as a fixed modification, while acetylation (protein N-terminal), oxidation (methionine), and lactylation (lysine) were set as variable modifications. The false discovery rate (FDR) thresholds for proteins, peptides, and PSMs were set to <1%.

4.14 Molecular dynamic simulation

The CKS1B structures were retrieved from Uniprot (https://www.uniprot.org/). CKS1B-K4lac was constructed using the “residue mutate” option in Discovery Studio Visualizer (https://www.3dsbiovia.com/). the MD simulation of CKS1B-WT and CKS1B-K4lac were performed using Gromacs 2019.6 program under constant temperature, constant pressure and periodic boundary conditions. Amber99SB all-atomic force field is applied, TIP3P water model. In the MD simulation process, all bonds involving hydrogen atoms are constrained by the LINCS algorithm, and the integral step is 2 fs. The electrostatic interaction is calculated using the Particle-mesh Ewald PME method. The non-bond interaction cutoff is set to 10 A and updated every 10 steps. The V-rescale temperature coupling method was used to control the simulated temperature of 300 K, and the Parrinello-Rahman method was used to control the pressure of 1 bar. Firstly, the steepest descent method is used to minimize the energy of the two systems to eliminate the too close contact between atoms. Then, NVT and NPT equilibria of 1 ns were simulated at 300 K respectively. Finally, the system was simulated with 50 ns MD, and the conformation was saved every 10 ps. The visualization of simulation results was completed by using Gromacs embedded program and PyMOL.

4.15 Protein–protein docking

The structures of CDK1-3 and p27 were predicted using AlphaFold Server (https://alphafoldserver.com/). The prepared structures were then used for molecular docking with the MOE 2024 program. Docking calculations were performed to generate multiple candidate complexes, and the optimal docking model was selected based on scoring criteria.

4.16 Statistical Analysis

Statistical analyses, including overall survival analysis, unpaired *t*-test, one-way ANOVA, Wilcoxon signed-rank test, Fisher's exact test, and chi-square test, were performed using GraphPad Prism 8.0.1 (GraphPad Software, San Diego, CA, USA). A *p*-value of less than 0.05 was considered statistically significant.

ACKNOWLEDGEMENTS

We would like to thank Jingjie PTM BioLab (Hangzhou) Co. Inc. for quantitative proteomic and lactylomic analysis assistance. This work was supported by 1.3.5 project for disciplines of excellence at West China Hospital, Sichuan University (ZYGD23030) and The Natural Science Foundation of Sichuan Province (2024NSFSC1892).

AUTHOR CONTRIBUTIONS

H.C., K.N., Y.L. and H.T. conceived and designed the study; H.C., M.Z., H.L. and J.L. performed in vivo experiments; H.C., J.W., X.T. and X.Z. conducted Co-IP and WB analyses; H.C. and X.Z. carried out the immunohistochemistry; H.C. and X.T. analyzed Co-IP and WB results; H.C., Y.L., J.L., and H.L. analyzed the data; H.C., Y.L., and J.L. wrote the draft; T.Y., K.N. and H.T. revised the manuscript.

Reference

1. Herrera B, Dooley S, Breitkopf-Heinlein K. Potential roles of bone morphogenetic protein (BMP)-9 in human liver diseases. *Int J Mol Sci* 2014, **15**(4)**:** 5199–5220.

2. Jiang QQ, Liu BB, Xu KS. New insights into BMP9 signaling in liver diseases. *Mol Cell Biochem* 2021, **476**(10)**:** 3591–3600.

3. Li Q, Gu X, Weng H, Ghafoory S, Liu Y, Feng T*, et al.* Bone morphogenetic protein-9 induces epithelial to mesenchymal transition in hepatocellular carcinoma cells. *Cancer Sci* 2013, **104**(3)**:** 398–408.

4. Chen H, Nio K, Yamashita T, Okada H, Li R, Suda T*, et al.* BMP9-ID1 signaling promotes EpCAM-positive cancer stem cell properties in hepatocellular carcinoma. *Mol Oncol* 2021, **15**(8)**:** 2203–2218.

5. Fendt SM. 100 years of the Warburg effect: A cancer metabolism endeavor. *Cell* 2024, **187**(15)**:** 3824–3828.

6. Zhang D, Tang Z, Huang H, Zhou G, Cui C, Weng Y*, et al.* Metabolic regulation of gene expression by histone lactylation. *Nature* 2019, **574**(7779)**:** 575–580.

7. Yang Z, Zheng Y, Gao Q. Lysine lactylation in the regulation of tumor biology. *Trends Endocrinol Metab* 2024, **35**(8)**:** 720–731.

8. Lv X, Lv Y, Dai X. Lactate, histone lactylation and cancer hallmarks. *Expert Rev Mol Med* 2023, **25:** e7.

9. Wang T, Ye Z, Li Z, Jing DS, Fan GX, Liu MQ*, et al.* Lactate-induced protein lactylation: A bridge between epigenetics and metabolic reprogramming in cancer. *Cell Prolif* 2023, **56**(10)**:** e13478.

10. Li H, Sun L, Gao P, Hu H. Lactylation in cancer: Current understanding and challenges. *Cancer Cell* 2024, **42**(11)**:** 1803–1807.

11. Lao Y, Jin Y, Wu S, Fang T, Wang Q, Sun L*, et al.* Deciphering a profiling based on multiple post-translational modifications functionally associated regulatory patterns and therapeutic opportunities in human hepatocellular carcinoma. *Mol Cancer* 2024, **23**(1)**:** 283.

12. Lu Y, Zhu J, Zhang Y, Li W, Xiong Y, Fan Y*, et al.* Lactylation-Driven IGF2BP3-Mediated Serine Metabolism Reprogramming and RNA m6A-Modification Promotes Lenvatinib Resistance in HCC. *Adv Sci (Weinh)* 2024, **11**(46)**:** e2401399.

13. Feng F, Wu J, Chi Q, Wang S, Liu W, Yang L*, et al.* Lactylome Analysis Unveils

Lactylation-Dependent Mechanisms of Stemness Remodeling in the Liver Cancer Stem Cells. *Adv Sci (Weinh)* 2024, **11**(38)**:** e2405975.

14. Wang L, Zeng T, Wang Y, Wang G, Yu W, Zhang J*, et al.* K90 lactylation orchestrates YAP nuclear sequestration by impairing binding with exportin CRM1 and enhances HCC malignancy. *Cancer Lett* 2024, **611:** 217386.

15. Hong H, Han H, Wang L, Cao W, Hu M, Li J*, et al.* ABCF1-K430-Lactylation promotes HCC malignant progression via transcriptional activation of HIF1 signaling pathway. *Cell Death Differ* 2025.

16. Pines J. Cell cycle: reaching for a role for the Cks proteins. *Curr Biol* 1996, **6**(11)**:** 1399–1402.

17. Liu Z, Fu Q, Lv J, Wang F, Ding K. Prognostic implication of p27Kip1, Skp2 and Cks1 expression in renal cell carcinoma: a tissue microarray study. *J Exp Clin Cancer Res* 2008, **27**(1)**:** 51.

18. Calvisi DF, Ladu S, Pinna F, Frau M, Tomasi ML, Sini M*, et al.* SKP2 and CKS1 promote degradation of cell cycle regulators and are associated with hepatocellular carcinoma prognosis. *Gastroenterology* 2009, **137**(5)**:** 1816–1826 e1811–1810.

19. Slotky M, Shapira M, Ben-Izhak O, Linn S, Futerman B, Tsalic M*, et al.* The expression of the ubiquitin ligase subunit Cks1 in human breast cancer. *Breast Cancer Res* 2005, **7**(5)**:** R737–744.

20. Zhan F, Colla S, Wu X, Chen B, Stewart JP, Kuehl WM*, et al.* CKS1B, overexpressed in aggressive disease, regulates multiple myeloma growth and survival through SKP2- and p27Kip1-dependent and -independent mechanisms. *Blood* 2007, **109**(11)**:** 4995–5001.

21. Huis In 't Veld PJ, Wohlgemuth S, Koerner C, Muller F, Janning P, Musacchio A. Reconstitution and use of highly active human CDK1:Cyclin-B:CKS1 complexes. *Protein Sci* 2022, **31**(2)**:** 528–537.

22. Iozzo M, Pardella E, Giannoni E, Chiarugi P. The role of protein lactylation: A kaleidoscopic post-translational modification in cancer. *Mol Cell* 2025, **85**(7)**:** 1263–1279.

23. Massague J. TGF-beta signal transduction. *Annu Rev Biochem* 1998, **67:** 753–791.

24. Morikawa M, Koinuma D, Tsutsumi S, Vasilaki E, Kanki Y, Heldin CH*, et al.* ChIP-seq reveals cell type-specific binding patterns of BMP-specific Smads and a novel binding motif. *Nucleic Acids Res* 2011, **39**(20)**:** 8712–8727.

25. Jatzlau J, Mendez PL, Altay A, Raaz L, Zhang Y, Mahr S*, et al.* Fluid shear stress-modulated chromatin accessibility reveals the mechano-dependency of endothelial SMAD1/5-mediated gene transcription. *iScience* 2023, **26**(9)**:** 107405.

26. Ramachandran A, Vizan P, Das D, Chakravarty P, Vogt J, Rogers KW*, et al.* TGF-beta uses a novel mode of receptor activation to phosphorylate SMAD1/5 and induce epithelial-to-mesenchymal transition. *Elife* 2018, **7**.

27. Mughal MJ, Bhadresha K, Kwok HF. CDK inhibitors from past to present: A new wave of cancer therapy. *Semin Cancer Biol* 2023, **88:** 106–122.

28. Yang L, Xue J, Yang Z, Wang M, Yang P, Dong Y*, et al.* Side effects of CDK4/6 inhibitors in the treatment of HR+/HER2- advanced breast cancer: a systematic review and meta-analysis of randomized controlled trials. *Ann Palliat Med* 2021, **10**(5)**:** 5590–5599.

29. Chen L, Liu S, Tao Y. Regulating tumor suppressor genes: post-translational modifications. *Signal Transduct Target Ther* 2020, **5**(1)**:** 90.

30. Lu Z, Hunter T. Ubiquitylation and proteasomal degradation of the p21(Cip1), p27(Kip1) and p57(Kip2) CDK inhibitors. *Cell Cycle* 2010, **9**(12)**:** 2342–2352.

31. Kossatz U, Vervoorts J, Nickeleit I, Sundberg HA, Arthur JS, Manns MP*, et al.* C-terminal phosphorylation controls the stability and function of p27kip1. *EMBO J* 2006, **25**(21)**:** 5159–5170.

32. Ganoth D, Bornstein G, Ko TK, Larsen B, Tyers M, Pagano M*, et al.* The cell-cycle regulatory protein Cks1 is required for SCF(Skp2)-mediated ubiquitinylation of p27. *Nat Cell Biol* 2001, **3**(3)**:** 321–324.

33. Bloom J, Pagano M. Deregulated degradation of the cdk inhibitor p27 and malignant transformation. *Semin Cancer Biol* 2003, **13**(1)**:** 41–47.

34. Pagano M. Control of DNA synthesis and mitosis by the Skp2-p27-Cdk1/2 axis. *Mol Cell* 2004, **14**(4)**:** 414–416.

35. Lee EK, Kim DG, Kim JS, Yoon Y. Cell-cycle regulator Cks1 promotes hepatocellular carcinoma by supporting NF-kappaB-dependent expression of interleukin-8. *Cancer Res* 2011, **71**(21)**:** 6827–6835.

36. Liu X, Zhao D. CKS1B promotes the progression of hepatocellular carcinoma by activating JAK/STAT3 signal pathway. *Anim Cells Syst (Seoul)* 2021, **25**(4)**:** 227–234.

37. Kang YS, Jeong EJ, Seok HJ, Kim SK, Hwang JS, Choi ML*, et al.* Cks1 regulates human hepatocellular carcinoma cell progression through osteopontin expression. *Biochem Biophys Res Commun* 2019, **508**(1)**:** 275–281.

38. Shi W, Huang Q, Xie J, Wang H, Yu X, Zhou Y. CKS1B as Drug Resistance-Inducing Gene-A Potential Target to Improve Cancer Therapy. *Front Oncol* 2020, **10:** 582451.

39. Wang X, Fan W, Li N, Ma Y, Yao M, Wang G*, et al.* YY1 lactylation in microglia promotes angiogenesis through transcription activation-mediated upregulation of FGF2. *Genome Biol* 2023, **24**(1)**:** 87.

40. Sun M, Zhang Y, Mao R, Chen Y, Liu P, Ye L*, et al.* MeCP2 Lactylation Protects against Ischemic Brain Injury by Transcriptionally Regulating Neuronal Apoptosis. *Adv Sci (Weinh)* 2025, **12**(21)**:** e2415309.

41. Mi K, Chen Z, He J, Jiang C, Xia Y, Peng J. P300-Mediated ARRB1 Lactylation Promotes Mitochondrial Dysfunction and Neuronal Apoptosis in Subarachnoid Hemorrhage Via Upregulating S100A9. *Neurochem Res* 2025, **50**(3)**:** 174.

42. Yang L, Niu K, Wang J, Shen W, Jiang R, Liu L*, et al.* Nucleolin lactylation contributes to intrahepatic cholangiocarcinoma pathogenesis via RNA splicing regulation of MADD. *J Hepatol* 2024, **81**(4)**:** 651–666.

43. Chen Y, Wu J, Zhai L, Zhang T, Yin H, Gao H*, et al.* Metabolic regulation of

homologous recombination repair by MRE11 lactylation. *Cell* 2024, **187**(2)**:** 294–311 e221.

44. Liu S, Cai J, Qian X, Zhang J, Zhang Y, Meng X*, et al.* TPX2 lactylation is required for the cell cycle regulation and hepatocellular carcinoma progression. *Life Sci Alliance* 2025, **8**(6).

45. Xu Y, Ma X, Ni W, Zheng L, Lin Z, Lai Y*, et al.* PKM2-Driven Lactate Overproduction Triggers Endothelial-To-Mesenchymal Transition in Ischemic Flap via Mediating TWIST1 Lactylation. *Adv Sci (Weinh)* 2024, **11**(47)**:** e2406184.

46. Fan M, Yang K, Wang X, Chen L, Gill PS, Ha T*, et al.* Lactate promotes endothelial-to-mesenchymal transition via Snail1 lactylation after myocardial infarction. *Sci Adv* 2023, **9**(5)**:** eadc9465.

47. Ma N, Wang L, Meng M, Wang Y, Huo R, Chang G*, et al.* D-sodium lactate promotes the activation of NF-kappaB signaling pathway induced by lipopolysaccharide via histone lactylation in bovine mammary epithelial cells. *Microb Pathog* 2025, **199:** 107198.

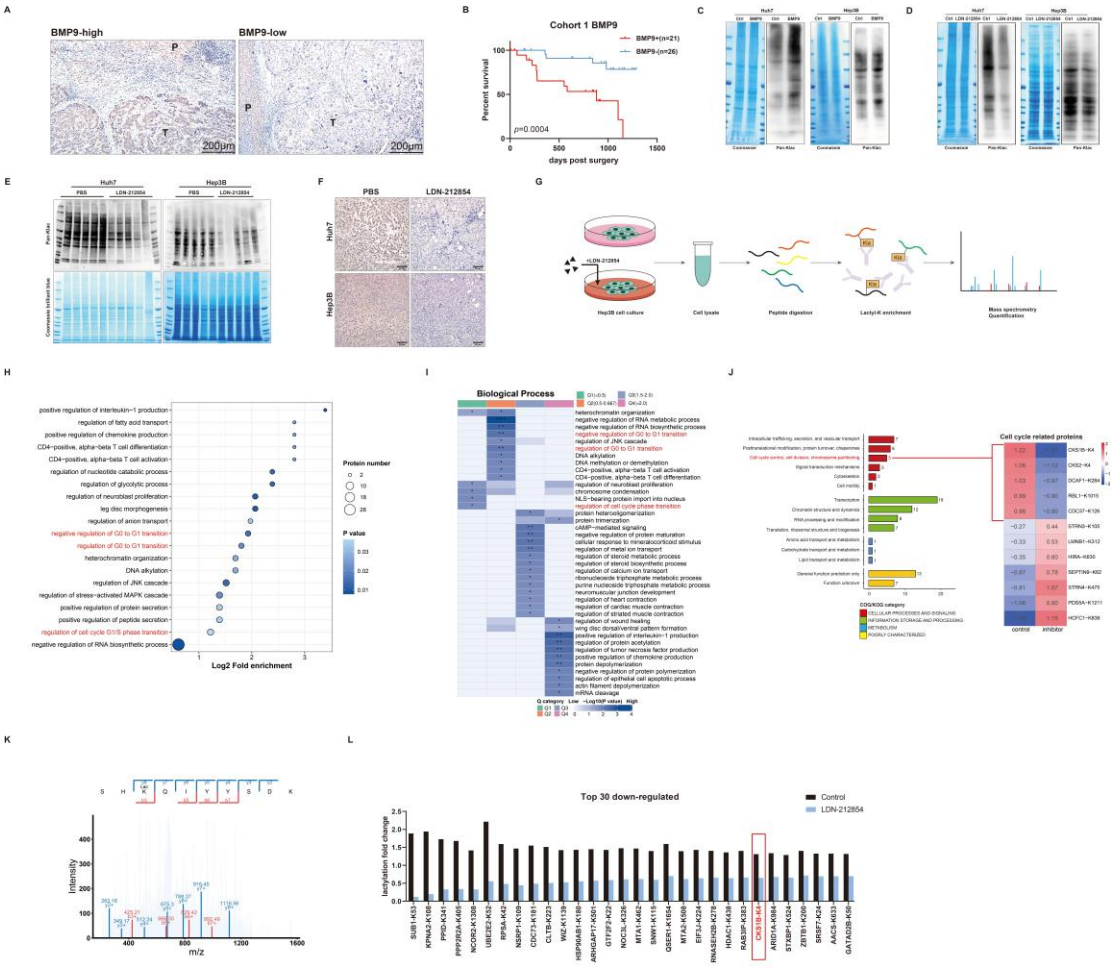
48. Zong Z, Ren J, Yang B, Zhang L, Zhou F. Emerging roles of lysine lactyltransferases and lactylation. *Nat Cell Biol* 2025, **27**(4)**:** 563–574.

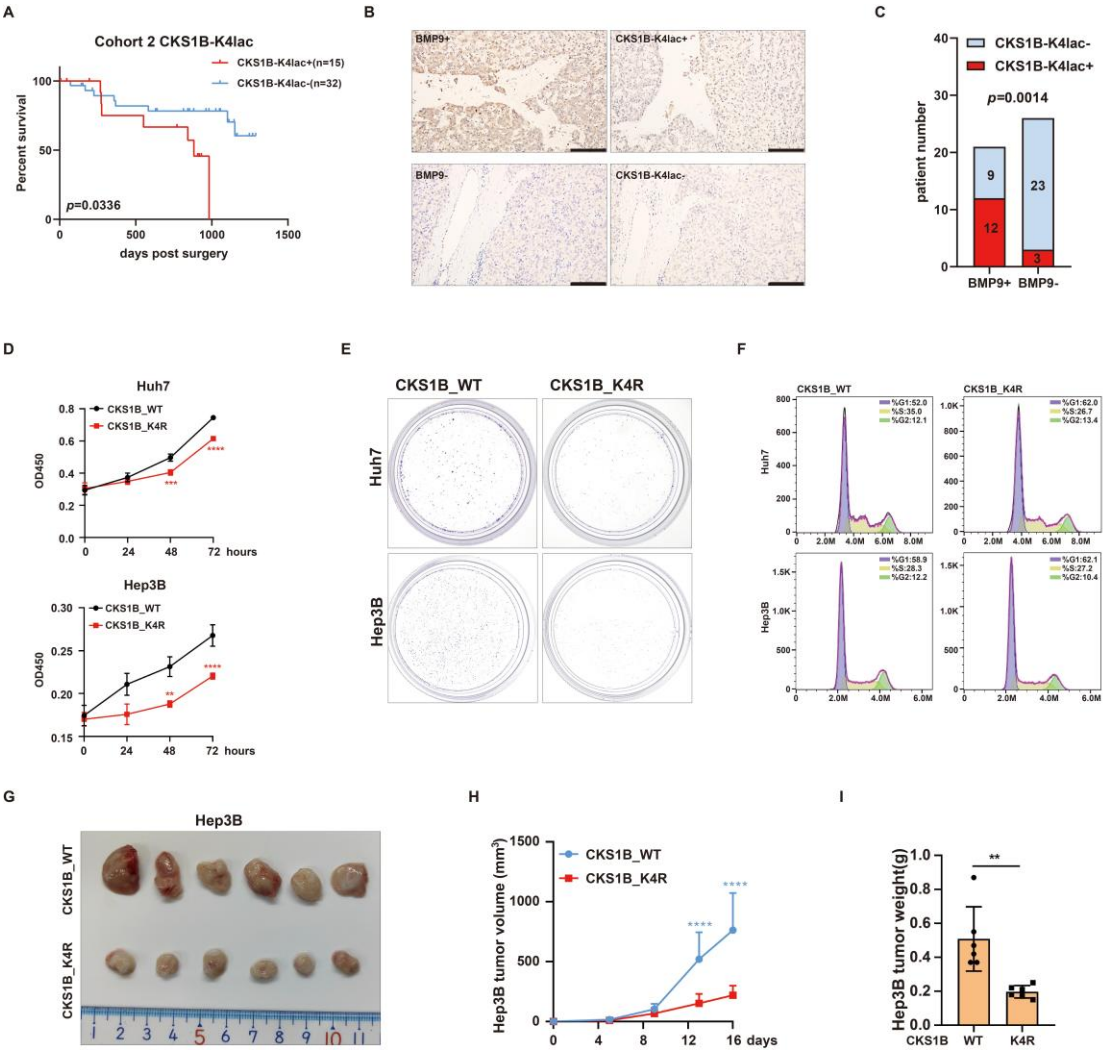
49. Li H, Liu C, Li R, Zhou L, Ran Y, Yang Q*, et al.* AARS1 and AARS2 sense L-lactate to regulate cGAS as global lysine lactyltransferases. *Nature* 2024, **634**(8036)**:** 1229–1237.

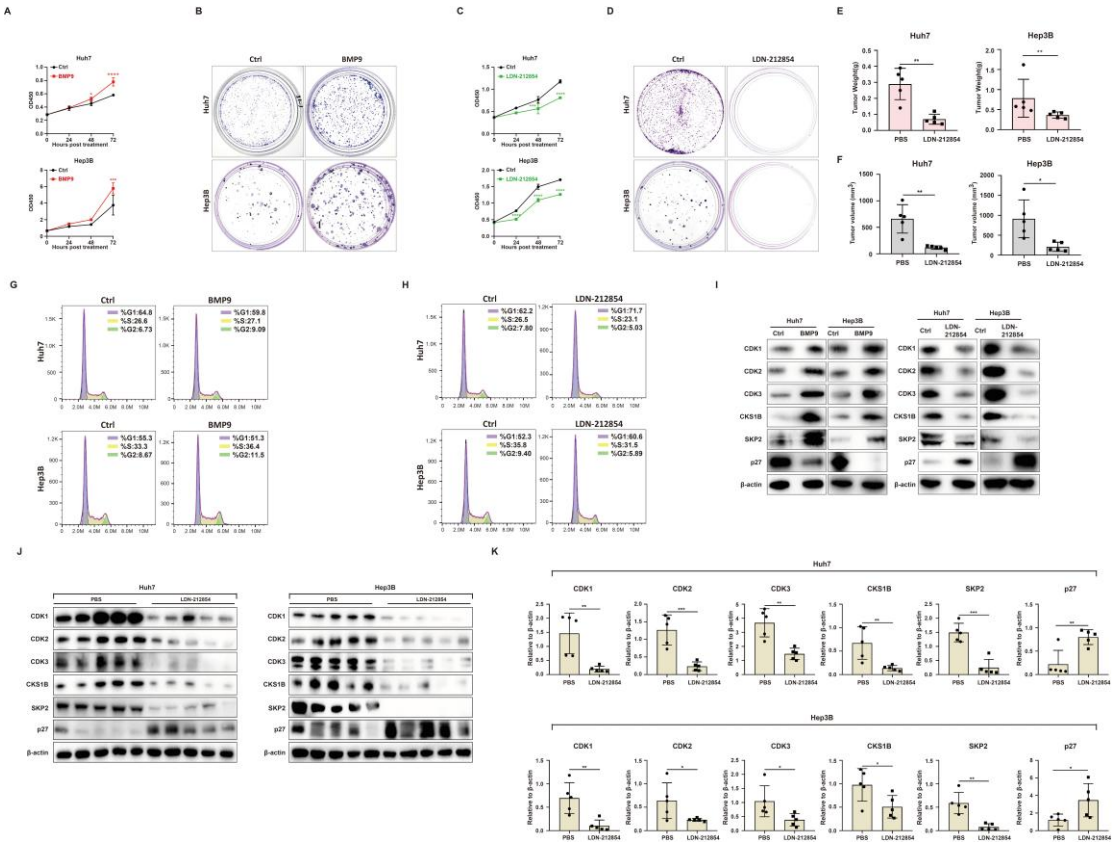
50. Ju J, Zhang H, Lin M, Yan Z, An L, Cao Z*, et al.* The alanyl-tRNA synthetase AARS1 moonlights as a lactyltransferase to promote YAP signaling in gastric cancer. *J Clin Invest* 2024, **134**(10).

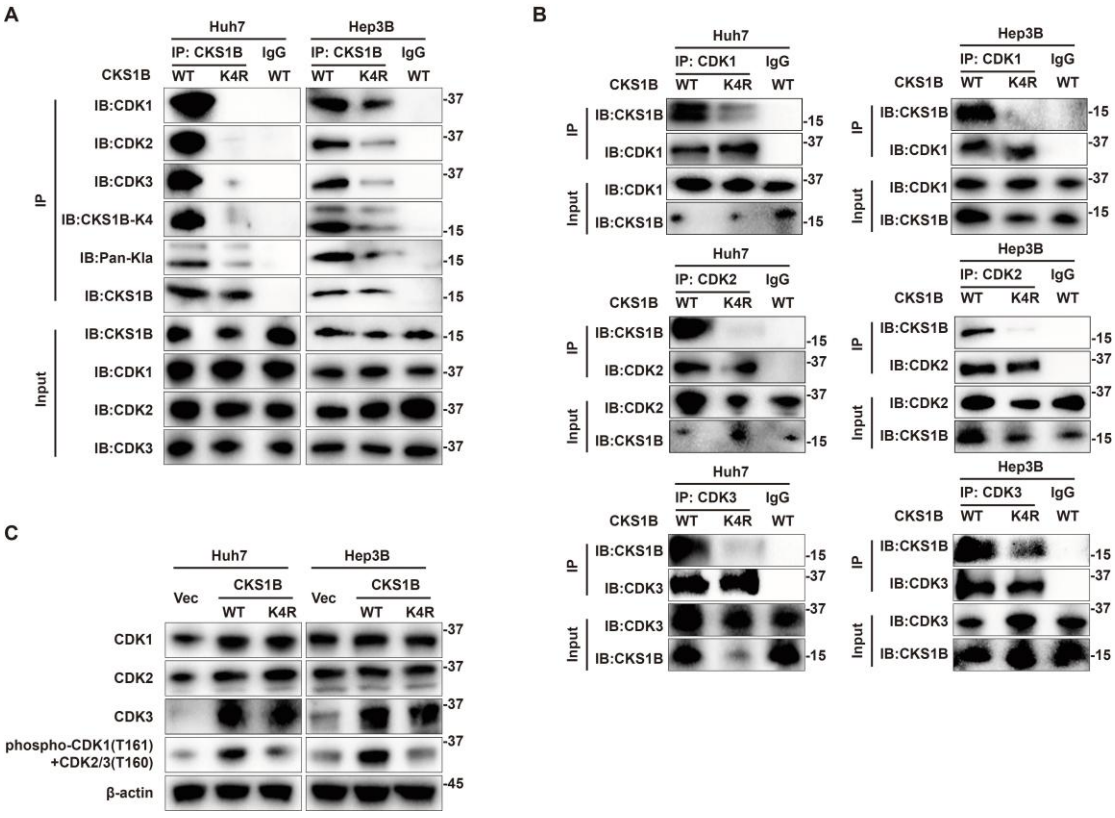
51. Zong Z, Xie F, Wang S, Wu X, Zhang Z, Yang B*, et al.* Alanyl-tRNA synthetase, AARS1, is a lactate sensor and lactyltransferase that lactylates p53 and contributes to tumorigenesis. *Cell* 2024, **187**(10)**:** 2375–2392 e2333.

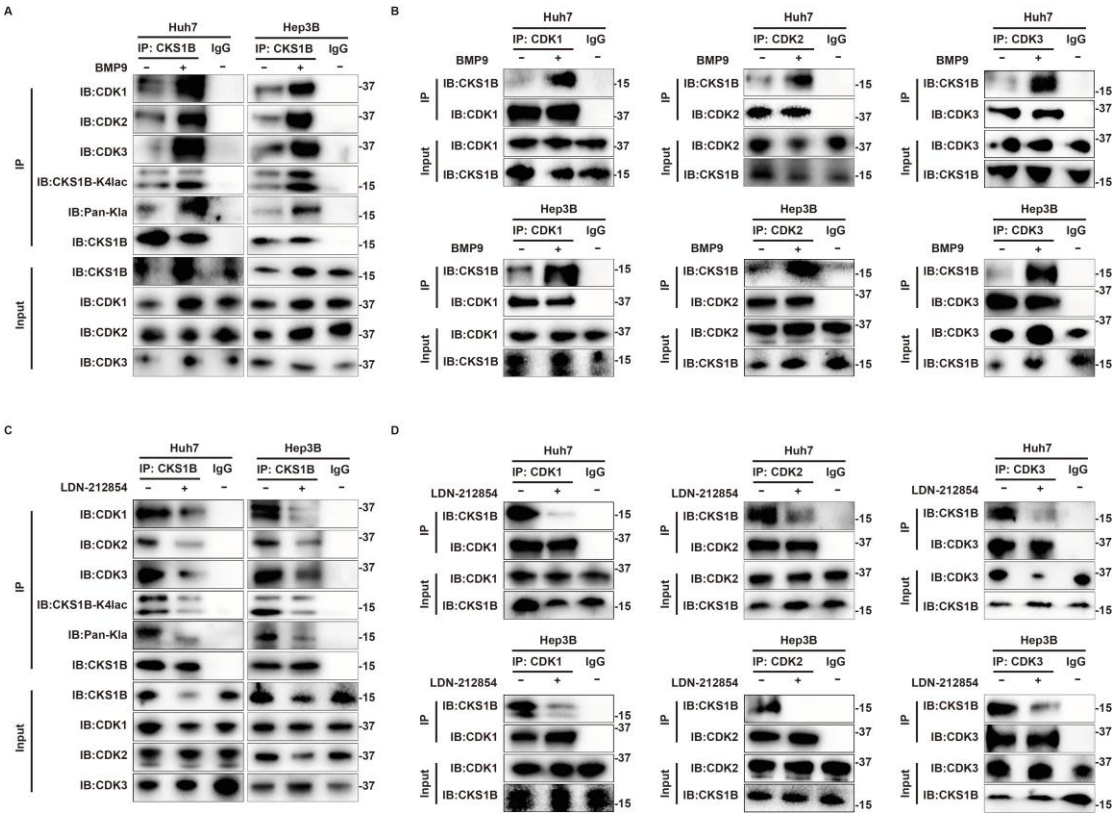
52. Li Z, Gong T, Wu Q, Zhang Y, Zheng X, Li Y*, et al.* Lysine lactylation regulates metabolic pathways and biofilm formation in Streptococcus mutans. *Sci Signal* 2023, **16**(801)**:** eadg1849.

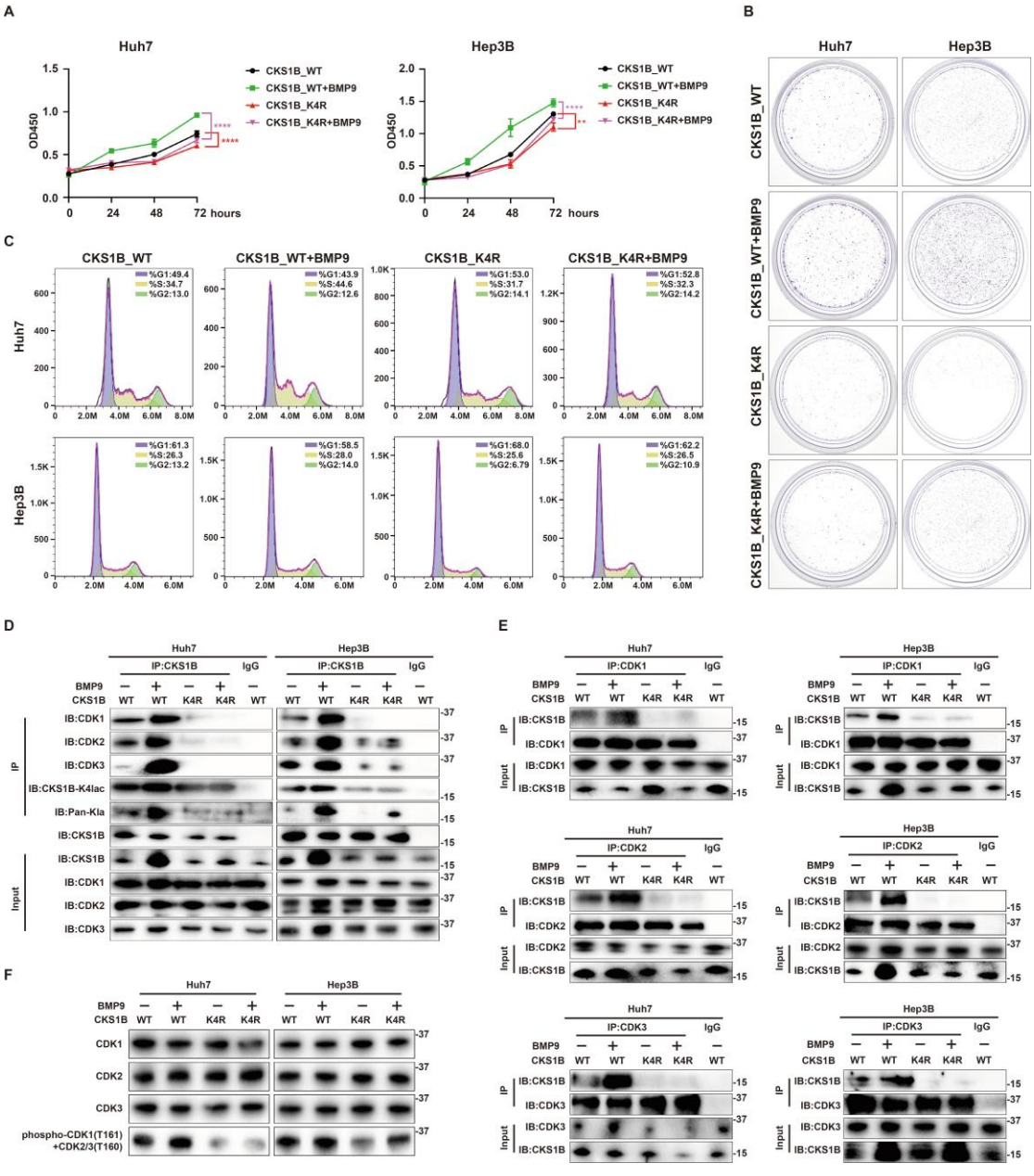

A
BMP9-high
BMP9-low
P
T
200μm
B
Cohort 1 BMP9
BMP9+(n=21)
BMP9-(n=26)
Percent survival
p=0.0004
days post surgery
C
D
E
Huh7
Hep3B
PBS
LDN-212854
Pan-Klac
Coomassie brilliant blue
F
PBS
LDN-212854
Huh7
Hep3B
G
+LDN-212854
Hep3B cell culture
Cell lysate
Peptide digestion
Lactyl-K enrichment
Mass spectrometry Quantification
H
positive regulation of interleukin−1 production
regulation of fatty acid transport
positive regulation of chemokine production
CD4−positive, alpha−beta T cell differentiation
CD4−positive, alpha−beta T cell activation
regulation of nucleotide catabolic process
regulation of glycolytic process
regulation of neuroblast proliferation
leg disc morphogenesis
regulation of anion transport
negative regulation of G0 to G1 transition
regulation of G0 to G1 transition
heterochromatin organization
DNA alkylation
regulation of JNK cascade
regulation of stress−activated MAPK cascade
positive regulation of protein secretion
positive regulation of peptide secretion
regulation of cell cycle G1/S phase transition
negative regulation of RNA biosynthetic process
Log2 Fold enrichment
Protein number
P value
I
Biological Process
heterochromatin organization
negative regulation of RNA metabolic process
negative regulation of RNA biosynthetic process
negative regulation of G0 to G1 transition
regulation of JNK cascade
regulation of G0 to G1 transition
DNA alkylation
DNA methylation or demethylation
CD4−positive, alpha−beta T cell activation
CD4−positive, alpha−beta T cell differentiation
regulation of neuroblast proliferation
chromosome condensation
NLS−bearing protein import into nucleus
regulation of cell cycle phase transition
protein heterooligomerization
protein trimerization
cAMP−mediated signaling
negative regulation of protein maturation
cellular response to mineralocorticoid stimulus
regulation of metal ion transport
regulation of steroid metabolic process
regulation of steroid biosynthetic process
regulation of calcium ion transport
ribonucleoside triphosphate metabolic process
purine nucleoside triphosphate metabolic process
neuromuscular junction development
regulation of heart contraction
regulation of cardiac muscle contraction
regulation of striated muscle contraction
regulation of wound healing
wing disc dorsal/ventral pattern formation
positive regulation of interleukin−1 production
regulation of protein acetylation
regulation of tumor necrosis factor production
positive regulation of chemokine production
protein depolymerization
negative regulation of protein polymerization
regulation of epithelial cell apoptotic process
actin filament depolymerization
mRNA cleavage
Q category
−Log10(P value)
J
Cell cycle related proteins
CKS1B-K4
CKS2-K4
DCAF1-K394
RBL1-K1015
CDC37-K126
STRN3-K105
UIMB1-K312
HIRA-K630
SEPTIN9-K62
STRN4-K475
PDS5A-K1211
HCFC1-K636
control
inhibitor
COG/KOG category
CELLULAR PROCESSES AND SIGNALING
INFORMATION STORAGE AND PROCESSING
METABOLISM
POORLY CHARACTERIZED
K
Intensity
m/z
L
Top 30 down-regulated
Control
LDN-212854
lactylation fold change
SUB1-K53
KPNA2-K198
PPID-K341
PPP2R2A-K466
NCOR2-K1368
UBE2E2-K52
RFSA-K42
NSEP1-K106
CDC73-K161
CLTB-K223
WIZ-K1139
HSPA9AB1-K186
ARHGAP17-K561
GTF3P2-K22
NOC3L-K326
MTA1-K462
SNW1-K115
QSER1-K1654
MTA2-K598
EFTJ-K224
RNASEH2B-K276
HDAC1-K439
RASSF8-K282
CKS1B-K4
ARID1A-K984
STXBP1-K324
ZBTB1-K290
SRSF7-K24
AACS-K633
GATAD2B-K50

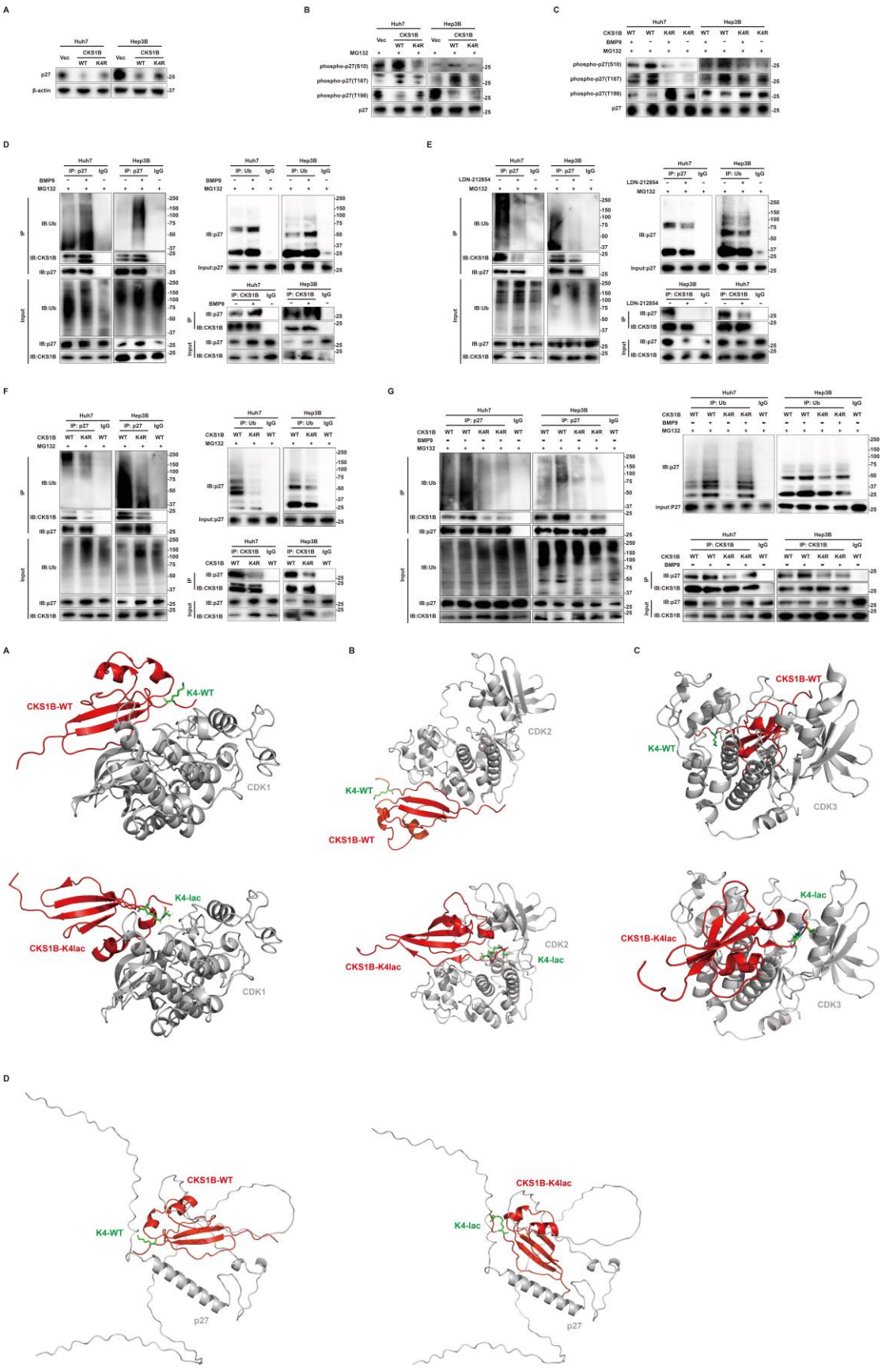

A
Cohort 2 CKS1B-K4lac
CKS1B-K4lac+(n=15)
CKS1B-K4lac-(n=32)
Percent survival
p=0.0336
days post surgery
B
BMP9+
CKS1B-K4lac+
BMP9-
CKS1B-K4lac-
C
CKS1B-K4lac-
CKS1B-K4lac+
p=0.0014
patient number
BMP9+ BMP9-
D
Huh7
CKS1B_WT
CKS1B_K4R
OD450
hours
Hep3B
E
CKS1B_WT
CKS1B_K4R
Huh7
Hep3B
F
CKS1B_WT
CKS1B_K4R
Huh7
Hep3B
G
Hep3B
CKS1B_WT
CKS1B_K4R
H
CKS1B_WT
CKS1B_K4R
Hep3B tumor volume (mm³)
days
I
Hep3B tumor weight(g)
CKS1B WT K4R

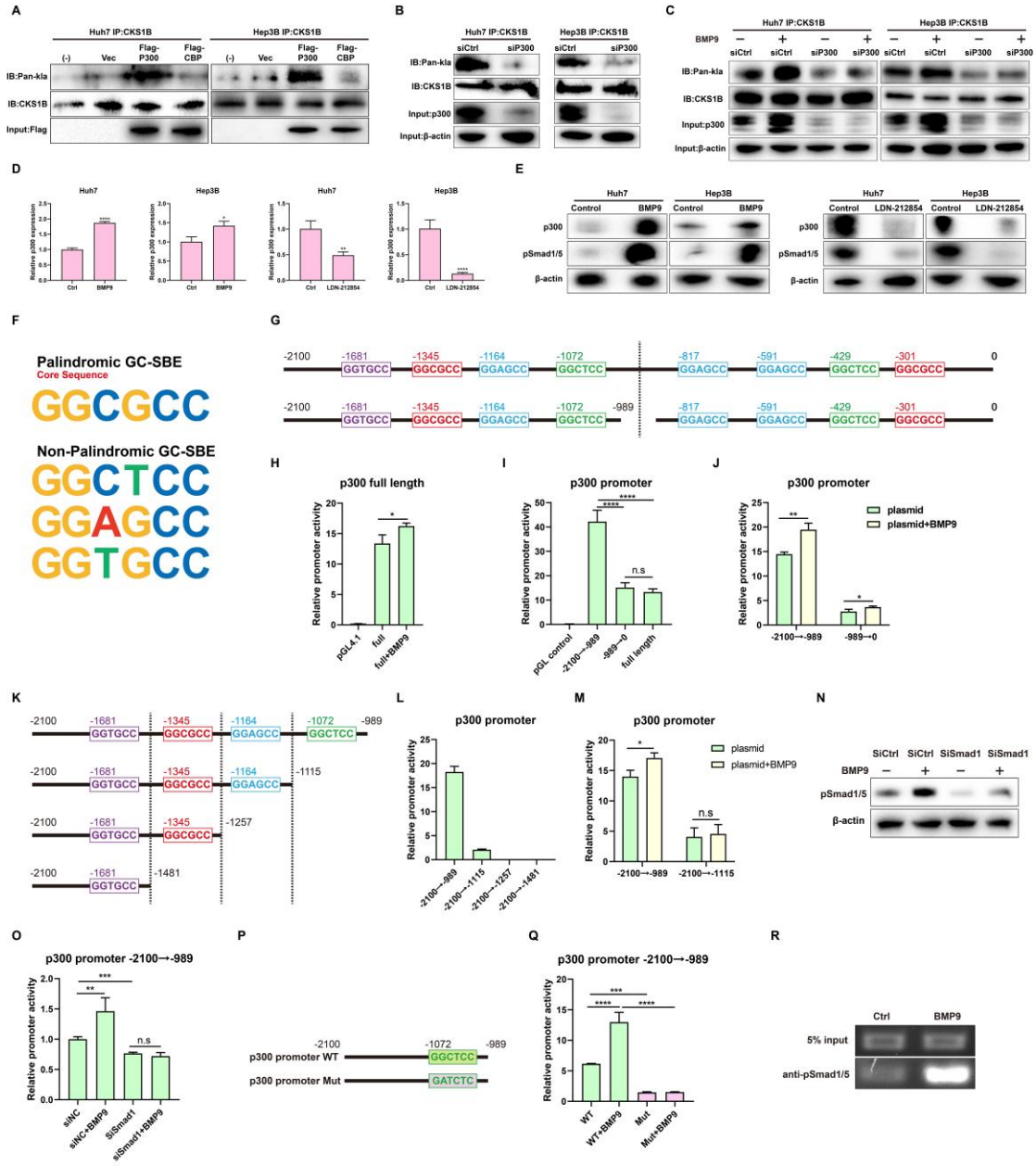

A
B
C
D
E
F
G
H
I
J
K
Huh7
Hep3B
Ctrl
BMP9
LDN-212854
PBS
Hours post treatment
Tumor Weight(g)
Tumor volume (mm³)
%G1:64.8
%S:26.6
%G2:6.73
%G1:59.8
%S:27.1
%G2:9.09
%G1:55.3
%S:33.3
%G2:8.67
%G1:51.3
%S:36.4
%G2:11.5
%G1:62.2
%S:26.5
%G2:7.80
%G1:71.7
%S:23.1
%G2:5.03
%G1:52.3
%S:35.8
%G2:9.40
%G1:60.6
%S:31.5
%G2:5.89
CDK1
CDK2
CDK3
CKS1B
SKP2
p27
β-actin
Relative to β-actin

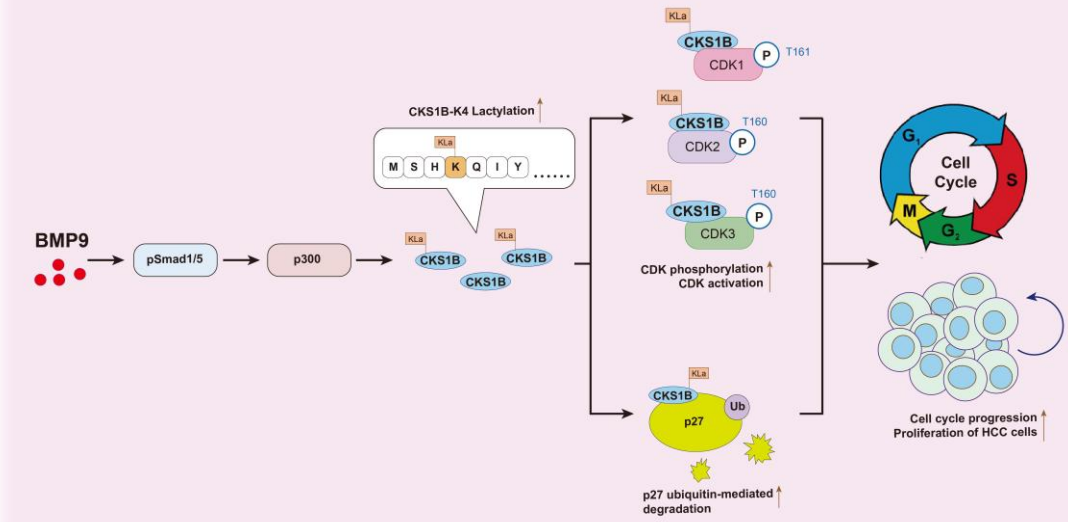

A
Huh7
Hep3B
IP: CKS1B
IgG
CKS1B
WT
K4R
IB:CDK1
IB:CDK2
IB:CDK3
IB:CKS1B-K4
IB:Pan-Kla
IB:CKS1B
IP
Input
B
IP: CDK1
IP: CDK2
IP: CDK3
C
Vec
phospho-CDK1(T161)
+CDK2/3(T160)
β-actin


A
Huh7
Hep3B
IP: CKS1B
IgG
BMP9
IP
Input
IB:CDK1
IB:CDK2
IB:CDK3
IB:CKS1B-K4lac
IB:Pan-Kla
IB:CKS1B
-37
-15
B
IP: CDK1
IP: CDK2
IP: CDK3
C
LDN-212854
D


A
Huh7
Hep3B
OD450
hours
CKS1B_WT
CKS1B_WT+BMP9
CKS1B_K4R
CKS1B_K4R+BMP9
B
Huh7
Hep3B
C
CKS1B_WT
CKS1B_WT+BMP9
CKS1B_K4R
CKS1B_K4R+BMP9
D
IP:CKS1B
IgG
BMP9
CKS1B
IB:CDK1
IB:CDK2
IB:CDK3
IB:CKS1B-K4lac
IB:Pan-Kla
IB:CKS1B
E
IP:CDK1
IP:CDK2
IP:CDK3
F
phospho-CDK1(T161)
+CDK2/3(T160)


A
Huh7
Hep3B
Vec
CKS1B
WT
K4R
p27
β-actin
B
MG132
phospho-p27(S10)
phospho-p27(T187)
phospho-p27(T198)
p27
C
CKS1B
BMP9
MG132
D
IP: p27
IgG
IP: Ub
IP: CKS1B
IB:Ub
IB:CKS1B
IB:p27
Input:p27
E
LDN-212854
F
G
Input:P27
A
CKS1B-WT
K4-WT
CDK1
CKS1B-K4lac
B
CDK2
C
CDK3
D
p27


A
Huh7 IP:CKS1B
Hep3B IP:CKS1B
(-)
Vec
Flag-P300
Flag-CBP
IB:Pan-kla
IB:CKS1B
Input:Flag
B
siCtrl
siP300
Input:p300
Input:β-actin
C
BMP9
D
Huh7
Hep3B
Ctrl
BMP9
LDN-212854
E
Control
p300
pSmad1/5
β-actin
F
Palindromic GC-SBE
Core Sequence
GGCGCC
Non-Palindromic GC-SBE
GGCTCC
GGAGCC
GGTGCC
G
-2100
-1681
-1345
-1164
-1072
-989
-817
-591
-429
-301
0
GGTGCC
GGCGCC
GGAGCC
GGCTCC
H
p300 full length
Relative promoter activity
pGL4.1
full
full+BMP9
I
p300 promoter
pGL control
-2100→-989
-989→0
full length
n.s
J
plasmid
plasmid+BMP9
-2100→-989
-989→0
K
-1115
-1257
-1481
L
M
-2100→-1115
-2100→-1257
-2100→-1481
N
SiCtrl
SiSmad1
pSmad1/5
β-actin
O
p300 promoter -2100→-989
siNC
siNC+BMP9
SiSmad1
siSmad1+BMP9
P
p300 promoter WT
p300 promoter Mut
GATCTC
Q
WT
WT+BMP9
Mut
Mut+BMP9
R
Ctrl
BMP9
5% input
anti-pSmad1/5


BMP9
pSmad1/5
p300
CKS1B-K4 Lactylation
M S H K Q I Y .....
KLa
CKS1B
CKS1B
CKS1B
KLa
CKS1B
CDK1
P
T161
CKS1B
CDK2
P
T160
CKS1B
CDK3
P
T160
CDK phosphorylation
CDK activation
CKS1B
Ub
p27
p27 ubiquitin-mediated
degradation
Cell
Cycle
G1
S
M
G2
Cell cycle progression
Proliferation of HCC cells

Supplementary Files

This is a list of supplementary files associated with this preprint. Click to download.

- SupplementaryTables.pdf
- SupplementaryFigurelegend.pdf
- AllWesternblotoriginalimages.pdf